

NUCLEATION OF OXIDE INCLUSIONS DURING  
THE SOLIDIFICATION OF IRON

by

GORDON EDWARD FORWARD

B.A.Sc, University of British Columbia  
(1960)

M.A.Sc, University of British Columbia  
(1962)

Submitted in Partial Fulfillment  
of the Requirements for  
the Degree of

Doctor of Science

at the

Massachusetts Institute of Technology

1966

Signature of Author  
Department of Metallurgy

Signature of Professor  
in Charge of Research

Signature of Chairman of  
Departmental Committee on  
Graduate Research

## ABSTRACT

NUCLEATION OF OXIDE INCLUSIONS DURING  
THE SOLIDIFICATION OF IRON

by

GORDON EDWARD FORWARD

Submitted to the Department of Metallurgy on May 13, 1966, in partial fulfillment of the requirements for the degree of Doctor of Science.

---

The processes by which oxide inclusions form during the solidification of iron melts have been investigated. Various mechanisms were considered and two solidification models simulating the possible processes were constructed. Model I assumes easy nucleation of the oxide phase and melt-oxide equilibrium throughout the freezing process. Little or no supersaturation of the solutes in the liquid occurs. Model II assumes homogeneous nucleation of the oxide phases resulting in large supersaturations of the interdendritic liquid. Critical supersaturations for homogeneous nucleation were calculated from classical nucleation theory as adapted by Turpin and Elliott. For the case of iron containing oxygen and silicon, the interfacial tensions used were;  $\sigma_{\text{Fe}_2 - \text{SiO}_2} = 1300 \text{ ergs/cm}^2$  and  $\sigma_{\text{Fe}_2 - \text{FeO}_2} = 250 \text{ ergs/cm}^2$ . For each model, inclusion compositions and their location in the solid section were determined.

Experiments were performed in which iron melts were equilibrated with silica crucibles then quenched. The ingots were sectioned, and the distributions of the inclusions noted. Inclusions were extracted and analyzed. The results were then compared to those predicted from Models I and II.

The locations and compositions of the inclusions observed from experiment agree with those determined from Model II. In all cases, oxide inclusions which formed during solidification of iron appeared at the primary dendrite boundaries corresponding to the last portion of the iron to solidify. Analysis of the inclusions showed that, in ingots containing less than 0.010 Wt% silicon, the inclusions are pure FeO. In the range 0.01 to 0.09 Wt % silicon the inclusions are mixed silicates, and above 0.09 Wt% silicon all oxygen is combined as glassy SiO<sub>2</sub>.

The results indicate that during the solidification of iron containing silicon and oxygen, large supersaturations of the interdendritic liquid occur. The distributions and compositions of the inclusions are consistent with those calculated from classical nucleation theory indicating that the nucleation of oxide inclusions during solidification is homogeneous, occurring in the liquid iron ahead of the advancing solid iron-liquid interface.

Thesis Supervisor: Professor John F. Elliott

Title: Professor of Metallurgy

TABLE OF CONTENTS

<u>Chapter Number</u>		<u>Page Number</u>
	ABSTRACT.....	ii
	LIST OF FIGURES.....	vi
	LIST OF TABLES.....	ix
	ACKNOWLEDGEMENTS.....	xi
I	INTRODUCTION.....	1
II	LITERATURE SURVEY.....	2
	A. On Non-metallic Inclusions.....	2
	B. Classical Nucleation Theory.....	5
III	OUTLINE OF THIS INVESTIGATION.....	11
	A. The Iron-Silicon-Oxygen System.....	13
	B. Model I, "Barrier-Free Solidification.....	22
	1. Solute Rejection during Freezing.....	22
	2. Method of Calculation.....	26
	3. Metallographic Interpretation.....	26
	C. Model II, "Barrier" Solidification.....	35
	D. Model III, "Barrier-Free" Solidification With Mobile Particles.....	44
IV	APPARATUS, EXPERIMENTAL MATERIALS AND PROCEDURE.....	45
	A. Description of Apparatus.....	45
	1. Gas Purification.....	45
	2. Experimental Apparatus.....	46
	B. Materials.....	48
	C. Experimental Procedure.....	48
V	RESULTS.....	51
	A. Optical Observations of Polished Sections..	54
	1. Series Ia - 1550 °C - Slow Quench.....	55
	2. Series Ib - 1550 °C - Fast Quench.....	63
	3. Series II - 1650 °C - Fast and Slow Quench.....	65
	4. Series II (Continued) - High Oxygen Ingots.....	70
	B. Identification of Inclusions.....	76
	1. Extraction and Chemical Analysis of Inclusions.....	76
	2. X-Ray Diffraction of Extracted Inclusions.....	80

<u>Chapter Number</u>		<u>Page Number</u>
	3. Electron Diffraction.....	80
	4. Electron Probe Analysis.....	82
VI	DISCUSSION.....	85
	A. Location of Inclusions.....	85
	B. Inclusion Compositions.....	89
	C. Isolation of Nucleation Sites During Solidification.....	91
	1. The Supercooling of Liquids.....	91
	2. Cooling of Liquid Iron.....	92
	3. Solidification of Iron.....	93
VII	SUMMARY AND CONCLUSIONS.....	94
VIII	SUGGESTIONS FOR FURTHER WORK.....	96
	REFERENCES.....	98
	APPENDIX A - CALCULATION OF LIQUID IRON COMPOSITIONS IN EQUILIBRIUM WITH UNSATURATED FeO-SiO <sub>2</sub> SLAGS.....	101
	APPENDIX B - CALCULATION OF FREEZING POINT LOWERING.....	103
	APPENDIX C - CHEMICAL ISOLATION AND ANALYSIS OF OXIDE INCLUSIONS. A. Procedure.....	104
	B. Discussion of Results.....	105
	APPENDIX D - X-RAY DIFFRACTION OF OXIDE RESIDUES.....	111
	APPENDIX E - LOT ANALYSIS OF ELECTROLYTIC IRON.....	112
	APPENDIX F - INCLUSION AREA COUNT.....	113
	BIOGRAPHICAL NOTE.....	114

LIST OF FIGURES

<u>Figure Number</u>		<u>Page Number</u>
1	Nucleation Lines for FeO and SiO <sub>2</sub> in Liquid Iron at 1536°C.....	8
2	Isothermal Section of the Fe-Si-O System - 1550°C.....	14
3	Isothermal Section of the Fe-Si-O System - 1535°C.....	15
4	Isothermal Section of the Fe-Si-O System - 1530°C.....	16
5	Isothermal Section of the Fe-Si-O System - 1500°C.....	17
6	Equilibrium Solubility Limits for Silicon and Oxygen in Liquid Iron.....	18
7	Schematic Three Dimensional Representation of the Iron-Rich Corner in the Fe-Si-O System.....	20
8	Solute Rejection During the Solidification of Iron - Silicon.....	24
9	Solute Rejection During the Solidification of Iron - Oxygen.....	25
10	Resulting Micrograph for Liquid A.....	28
11	Resulting Micrograph for Liquid B.....	29
12	Resulting Micrograph for Liquid C.....	30
13	Resulting Micrograph for Liquid D.....	31
14	Resulting Micrograph for Liquid E.....	32
15	Summary of Liquid Composition Changes During "Barrier-Free" Solidification.....	33
16	Resulting Micrograph for Liquid A.....	37
17	Resulting Micrograph for Liquid B.....	38

<u>Figure Number</u>		<u>Page Number</u>
18	Resulting Micrograph for Liquid C.....	39
19	Resulting Micrograph for Liquid D.....	40
20	Resulting Micrograph for Liquid E.....	41
21	Summary of Liquid Composition Changes During " Barrier" Solidification.....	43
22	Gas Purification System.....	45
23	Reaction Chamber.....	47
24	Plan Section of an Ingot Showing Allocations of Portions for Analysis.....	50
25	Evaluation of $f_s$ .....	54
26	FeO type Inclusions in Ingot 99; 0.006 Wt% Si.....	56
27	Silica Type Particle in an Iron Matrix.....	57
28	Sections Through a Rosette Type Inclusion.....	58
29	Cell Boundary Precipitates in Ingots With Greater than 0.010 Wt% Si - Ingot 52..	60
30	Rod-Like Grain Boundary Inclusions - Ingot 53; 0.012 Wt% Si.....	61
31	Origin of Rod-Type Eutectic.....	62
32	Inclusions Type as a Function of Quench Rate - Ingot 107; 0.005 Wt% Si.....	64
33	Time - Temperature Profiles Showing the Quench Sequences for Runs 126 and 127.....	66
34	Fast Quench from 1550°C - Ingot 125; 0.160 Wt% Si.....	67
35	Fast Quench from 1550°C - Ingot 126; 0.087 Wt% Si.....	68

<u>Figure Number</u>		<u>Page Number</u>
36	Slow Cool from 1650°C to 1538°C, Fast Quench from 1538°C - Ingot 127; 0.21 Wt% Si.....	68
37	Silica Inclusions at Top of Ingot 127; 0.21 Wt% Si.....	69
38	Complex Random Inclusion Appearing In High Oxygen Ingots Quenched from 1650°C - Ingot 119; 0.025 Wt% Si.....	70
39	Cooling and Solidification of Melts Originally at Silica Saturation - 1650°C.....	72
40	Cooling and Solidification of Liquid Slag "L".....	72
41	Results of Chemical Analysis of Inclusions Extracted from Ingots Quenched from 1550°C...	77
42	Percentage of Total Oxygen Combined as SiO <sub>2</sub> as a Function of the Silicon Content of the Ingots.....	79
43	X-Ray Diffraction Patterns of Extracted Inclusions from Ingots 103, 109 and 106.....	81
44	Electron Diffraction Pattern of FeO Inclusions from Ingot 103.....	82
45	Electron Probe Trace for Si K Radiation Across Inclusions in Ingot 108; 0.008 Wt% Si.....	83
46	Electron Probe Trace for Si K Radiation Across Inclusions in Ingot 105; 0.04 Wt% Si.....	84
C-1	Estimation of Amount of "Extraneous" Iron in Oxide Residues.....	109



LIST OF TABLES

<u>Table Number</u>		<u>Page Number</u>
1	Model I, Liquid A; Initial Composition Si = 0.20 %, O = 0.0059 %.....	28
2	Model I, Liquid B; Initial Composition Si = 0.10 %, O = 0.008 %.....	29
3	Model I, Liquid C; Initial Composition Si = 0.040 %, O = 0.013 %.....	30
4	Model I, Liquid D; Initial Composition Si = 0.010 %, O = 0.025 %.....	31
5	Model I, Liquid E; Initial Composition Si = 0.0015 %, O = 0.061 %.....	32
6	Model II, Liquid A; Initial Composition Si = 0.20 %, O = 0.0059 %.....	37
7	Model II, Liquid B; Initial Composition Si = 0.10 %, O = 0.008 %.....	38
8	Model II, Liquid C; Initial Composition Si = 0.040 %, O = 0.013 %.....	39
9	Model II, Liquid D; Initial Composition Si = 0.010 %, O = 0.025 %.....	40
10	Model II, Liquid E; Initial Composition Si = 0.0015 %, O = 0.061 %.....	41
11	Summary of Optical Observations on Quenched Specimens for Series Ia - 1550 °C - Slow Quench (H <sub>2</sub> Jets).....	73
12	Summary of Optical Observations on Quenched Specimens for Series Ib - 1550 °C - Fast Quench (Copper Plug).....	74
13	Summary of Optical Observations on Quenched Specimens for Series II - 1650°C..	75
14	Compositions of Inclusions as Determined by Calculation and by Experiment.....	89

<u>Table Number</u>		<u>Page Number</u>
C-1	Results of Extraction and Analysis of Inclusions.....	106
F-1	Results of Inclusions Counts for Ingots 125, 126 and 127 Performed on a Quantitative Television Microscope.....	113

ACKNOWLEDGMENTS

The author wishes to express his sincere appreciation to Professor John F. Elliott for his helpful guidance and encouragement throughout this study.

The following persons who have contributed to the successful completion of this project are also gratefully acknowledged:

Professor John Chipman and Dr. T. R. Meadowcroft for their interest and helpful suggestions;

Mr. Walter W. Correia for his assistance in the experimental portion of this investigation;

Mr. Theodore Strow for his assistance in chemical analyses;

My wife, Heather, for her preparation of the manuscript.

The American Iron and Steel Institute for their financial support of this project.

## I. INTRODUCTION

The processes by which non-metallic inclusions form during cooling and solidification of steel are not well understood. Over the past years investigators have accumulated an abundance of information concerning the nature, the compositions and the kinetics of formation of inclusions appearing in particular steels. For the most part these studies were performed on multicomponent systems under loosely controlled conditions, and thus, from the observation and identification of the end product, one could say very little about the processes by which an inclusion nucleated and grew.

The purpose of this investigation was to precipitate inclusions under carefully controlled conditions in a simple ternary system -- iron-silicon-oxygen. The thermodynamics of this system are well known and the compositions of the oxide phases found in the melt could be determined. A series of solidification experiments was performed from which the nature of nonmetallic inclusions could be related to the conditions at the time of their formation. In this manner an evaluation of the nucleation processes was obtained.

## II. LITERATURE SURVEY

### A. On Non-metallic Inclusions

Several excellent summaries of work performed on non-metallic inclusions are available in the literature<sup>1-5</sup>. Only those investigations related to this study, and in particular the Fe-Si-O system, are mentioned here.

A number of investigators in the past were not content merely to observe and catalogue inclusion types but attempted to explain the origin of these particles. One of the first attempts was that by Benedicts and Lofquist<sup>6</sup> who distinguished between "exogenous" inclusions, or those trapped mechanically in the melt, and "endogenous" inclusions, or those precipitated in the bath. Herty<sup>7</sup> recognized the importance of a knowledge of phase equilibria in explaining the origin of inclusions and painstakingly constructed from experiment relevant binary oxide phase diagrams. After comparing microstructures and compositions of observed inclusions with those of slags used in construction of the binary diagrams, he postulated mechanisms by which the inclusions were formed.

Hilty and Crafts<sup>8</sup> extended this type of analysis to ternary systems. They constructed the ternary equilibrium diagrams for the system Fe-O-S from experiment then considered the solidification of iron containing various amounts of sulphur and oxygen. The inclusions were classified as types I, II or III depending on the initial S/O ratio in the liquid

and hence on the ternary composition path followed by the liquid during the solidification of iron.

The first systematic investigations of inclusion types formed in the Fe-Si-O system were probably "by-products" of studies in which the solubility of oxygen in liquid iron containing silicon was of principal interest<sup>9-11</sup>. Ingots from the equilibrium studies were sectioned and the types and distributions of the inclusions noted. In each study it was observed that inclusion types were a function of the silicon content of the iron. In general, round grey FeO type particles were observed in ingots containing less than about 0.01 Wt% silicon whereas clear and glassy inclusions, thought to be pure silica, were present in ingots containing greater than 0.10 Wt% silicon. Mixed silicates were observed in the intermediate range and their character related to known phase equilibria in the FeO-SiO<sub>2</sub> binary system.

The extraction and identification of these inclusions has yielded much valuable information<sup>12,13</sup>. Unfortunately the extraction processes are often long and complicated, and in many cases certain of the oxide phases, principally FeO, dissolve to some extent leaving quantitative evaluations of inclusion content in question. Perhaps the most complete study of inclusion compositions and structures in the Fe-Si-O system using an extraction technique was that by Evans and Sloman<sup>14</sup>. They equilibrated pure iron samples weighing 300 - 400 grams in silica crucibles at 1600°C, then quenched,

sectioned, analyzed and examined the specimens. Inclusions were extracted by an alcohol-iodine solution then analyzed chemically and the phases identified by X-Ray diffraction. In the intermediate silicon range, 0.01 to 0.10 Wt% silicon, complex inclusions consisting of two immiscible glasses, or fayalite together with magnetite and wustite were identified.

Fisher and Wahlster<sup>15</sup> examined the kinetics of formation of oxide products during the deoxidation of iron containing 0.07 Wt% Oxygen. Probe samples taken periodically after the addition of silicon revealed the range of inclusion types mentioned above. The character and compositions of the inclusions were related to the silicon and oxygen contents of the bath at the time of sampling.

Quench methods were also observed to affect inclusion appearance. Sims<sup>10</sup> noted that, for melts quenched from a given temperature, the inclusion size decreased with increasing quench rate. Fisher and Wahlster observed that melts quenched from higher temperatures contained larger inclusions. These observations indicated that the nature of inclusions can in part be related to the thermal history of the quenched specimen.

In some cases investigators have recognized that the character of inclusions depends upon whether the inclusions were formed upon cooling of the liquid or during the solidification process. Elity<sup>9</sup>, for example, observed long, glassy "wishbones" of silica extending from spherical silica

particles that he had extracted from iron. He postulated that the sphere had formed during cooling and that the arms were formed as a metal-silica eutectic in the last of the liquid to solidify. More recently, Turkdogan<sup>16</sup> has examined the formation of deoxidation products during solidification and has attempted to predict inclusion behavior from current solidification theory and the available thermodynamic data.

Currently, there are two schools of thought concerning the mechanisms by which inclusions nucleate in iron. Firstly, there are those who contend that during cooling and solidification of liquid iron there are sufficient nuclei and/or substrates upon which a non-metallic phase may nucleate and grow, so that little or no supersaturation of the melt occurs. Equilibrium between the melt and the precipitating non-metallic phase is maintained at all times. There is a second possibility. Under certain conditions the liquid iron may be void of such nucleating agents and the non-metallic phase may not precipitate until supersaturations necessary for homogeneous nucleation are achieved. The later possibility has been considered by Turpin and Elliott<sup>17</sup>. Their analysis is examined in detail in the following section.

### B. Classical Nucleation Theory

Turpin and Elliott have treated the formation of non-metallic particles in liquid iron in terms of classical nucleation theory. More complex nucleation theories such as that by Cahn and Hilliard<sup>18</sup> are available, however detailed



information of the system is insufficient to support this type of treatment.

They propose, on the basis of classical theory, that the work to form a spherical nucleus is

$$W = 4\pi r^2 \sigma + \frac{4}{3} \pi r^3 \frac{\Delta G}{v} \quad (1)$$

where  $\sigma$  is the interfacial tension between the matrix and the new phase;  $r$  is the radius of the particle;  $\Delta G$  is the difference in the Gibbs free energy between the matrix and the new phase in massive form and  $v$  is the molar volume of the new phase. It is assumed that because the process takes place in a liquid medium that the strain energy term may be neglected. The critical radius,  $r^*$ , is the radius of the smallest cluster of molecules of the new phase that will grow spontaneously:

$$r^* = - \frac{2\sigma v}{\Delta G} \quad (2)$$

The related work,  $w^*$ , to form this nucleus is

$$w^* = \frac{(16\pi\sigma^3 v^2)}{3(\Delta G)^2} \quad (3)$$

The rate of formation homogeneously of nuclei per cubic centimeter of metal per second,  $I$ , is

$$I = A \exp \frac{-\Delta G_{\text{hom}}^*}{kT} \quad (4)$$

Where  $A$  is the frequency factor as defined by Turnbull and Fischer<sup>19</sup>,  $k$  is Boltzmann's constant,  $T$  is the temperature ( $^{\circ}\text{K}$ ),  $\Delta G_{\text{hom}}^*$  is the minimum work required to form the critical

nucleus homogenously in the melt.

Turpin and Elliott used these relationships to calculate the supersaturation of silicon and oxygen dissolved in liquid iron required to homogeneously nucleate liquid FeO and solid SiO<sub>2</sub> at 1536 °C. They proposed that the onset of nucleation occurs when the rate of formation of nuclei, I, is 1 nucleus per cubic centimeter per second - the results of the analysis are insensitive to the choice of this value in the range of  $I \times 10^4$ . The frequency factor, A, was estimated to be; for FeO,  $10^{30}$  and SiO<sub>2</sub>,  $10^{28}$ . The molar volumes were, for FeO<sub>1</sub>, 16 cm<sup>3</sup> / g.mole and for SiO<sub>2</sub>, 25 cm<sup>3</sup> / g.mole. Little is known of the interfacial tensions between the melt and the oxides so various values were used. They were;

$$\begin{aligned} \sigma_{\text{Fe}_1 - \text{FeO}_1} &= 250 \text{ and } 500 \text{ ergs / cm}^2, \text{ and} \\ \sigma_{\text{Fe}_1 - \text{SiO}_2} &= 1000, 1300 \text{ and } 1500 \text{ ergs / cm}^2. \end{aligned}$$

The supersaturations of oxygen and silicon required to nucleate the phases were then determined from the calculated value of  $\Delta G_{\text{crit}}^{\text{hom}}$ , which is the difference in free energy of a melt with a composition in equilibrium with the bulk oxide phase with that in local equilibrium with the oxide nucleus.

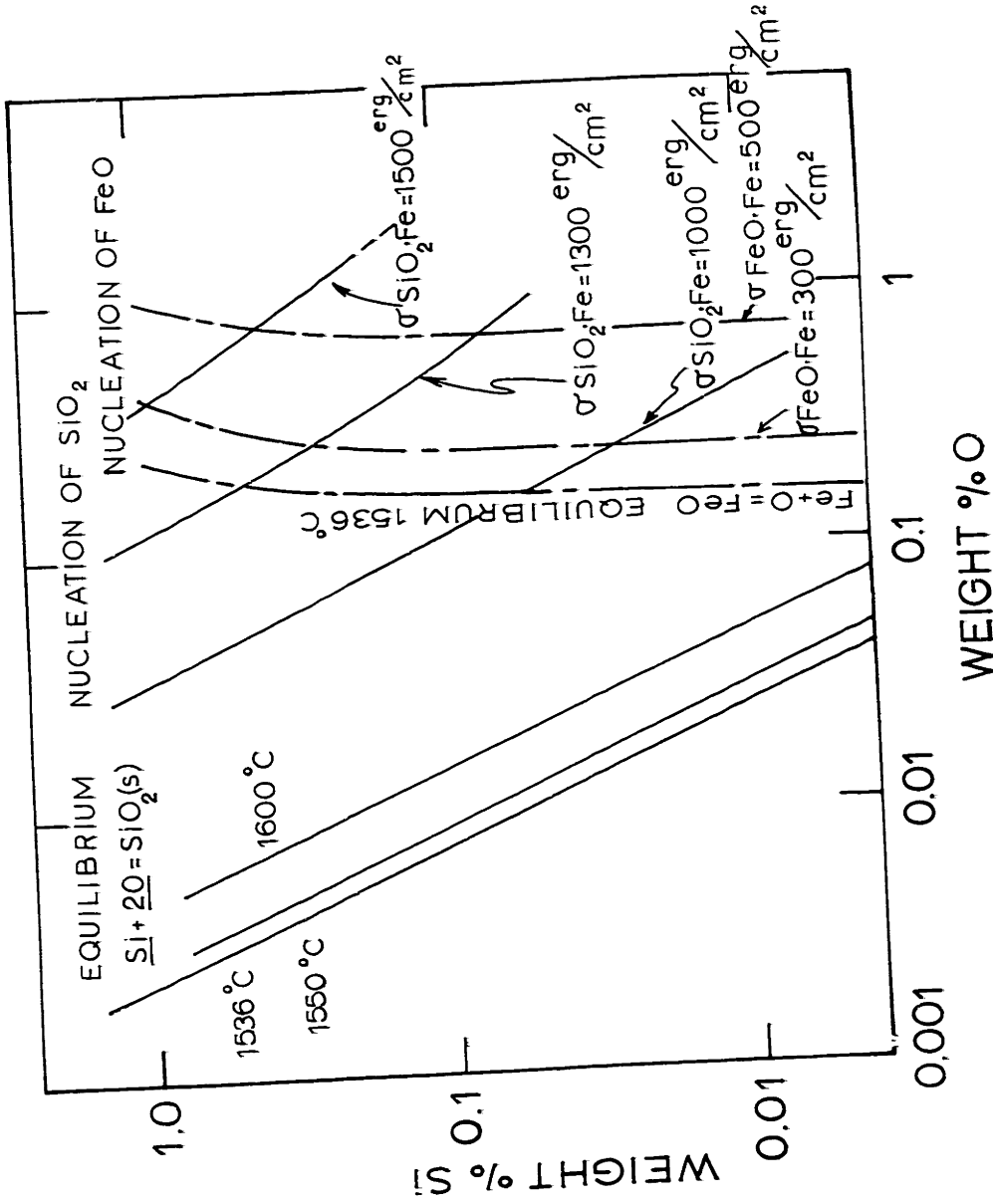
For FeO<sub>1</sub>

$$\Delta G_{\text{crit}}^{\text{hom}} = - RT \ln(f_{\text{O}} \cdot \%O) - \ln(f_{\text{O}} \cdot \%O)_{\text{eq}} \quad (5)$$

and for SiO<sub>2</sub>

$$\begin{aligned} \Delta G_{\text{crit}}^{\text{hom}} = - RT \ln(f_{\text{O}} \cdot \%O)^2 \times (f_{\text{Si}} \cdot \%Si) - \\ \ln(f_{\text{O}} \cdot \%O)_{\text{eq}}^2 \times (f_{\text{Si}} \cdot \%Si)_{\text{eq}} \quad (6) \end{aligned}$$

The results of this analysis are shown in Figure 1.



Effect of Interfacial Tension and Melt Composition on the Formation of Inclusions in the Iron-Silicon-Oxygen System

FIGURE 1

The equilibrium line in Figure 1 shows the composition of the Fe-O-Si melt which is in equilibrium with  $\text{SiO}_2$ . The dashed "nucleation lines for  $\text{SiO}_2$ " show the compositions of the melt at  $1536^\circ\text{C}$  necessary to reach  $\Delta G_{\text{crit}}^{\text{hom}}$  where nucleation of  $\text{SiO}_2(\text{s})$  can occur. The heavy lines show the composition of the melt necessary to obtain sufficient supersaturation with regard to oxygen to nucleate  $\text{FeO}_\ell$ .

During the solidification of an iron liquid whose initial composition rests somewhere on the silica equilibrium line, the composition of the liquid will increase in solute content moving to the right across the diagram until one or other of the nucleation barriers is crossed. The Figure shows that  $\text{FeO}_\ell$  will nucleate before  $\text{SiO}_2(\text{s})$  at low silicon levels in the Fe-Si-O system. The approximate upper limits of silicon content for this to occur as determined by the respective interfacial tensions are given by the intersections of the appropriate lines in Figure 1.

### III. OUTLINE OF THIS INVESTIGATION

There are two theories concerning the mechanisms by which inclusions may nucleate during the solidification of iron. They are:

a. Nucleation is heterogeneous, occurring on appropriate substrates. Little or no supersaturation of the liquid is necessary.

b. Nucleation is homogeneous, requiring large supersaturations in the liquid.

The aim of the present study was to obtain experimental evidence the analysis of which would provide a basis for the choice of mechanism.

The investigation carried out in the Fe-Si-O system was organized as follows:

1. Equilibrium phase diagrams for the ternary system Fe-Si-O were constructed from available thermodynamic data.

2. Using these diagrams the process of solidification of iron melts containing dissolved silicon and oxygen was considered. It was assumed that nucleation of the oxide phase was heterogeneous and that the oxide was at all times in equilibrium with the melt. The compositions and quantities of the oxide products and the composition of the interdendritic liquid were calculated as a function of the fraction of iron solidified.- Model I, "Barrier Free" Solidification.

3. The process of solidification of iron was considered in which homogeneous nucleation of inclusions was assumed. Using Turpin's calculated critical supersaturations and the above mentioned equilibrium diagrams the distributions and compositions of the oxide end product were calculated - Model II, "Barrier" Solidification.

4. Experiments were performed in which iron melts were equilibrated in silica crucibles at a temperature just above the melting point of iron. The samples were quenched and the ingots were sectioned, analyzed and examined for inclusions. The experimental results were compared to those calculated for each of the aforementioned models and in this way the nucleation phenomenon was evaluated.

#### A. THE IRON-SILICON-OXYGEN SYSTEM

To assist in the analysis and interpretation of oxide products formed during the cooling and solidification of iron melts containing silicon and oxygen, an Fe-Si-O equilibrium diagram on the iron side of the FeO-SiO<sub>2</sub> binary was constructed. The related binaries are well known,<sup>20,21,22,23</sup> and considerable equilibrium data exist for the iron-rich corner of the ternary system. The following schematic diagrams, Figures 2, 3, 4 and 5, are a series of isothermal sections of the ternary system as constructed from the available information on the phase diagrams. Because of the very limited solubility of oxygen in liquid iron, the scale in the iron-rich corner has been greatly exaggerated.

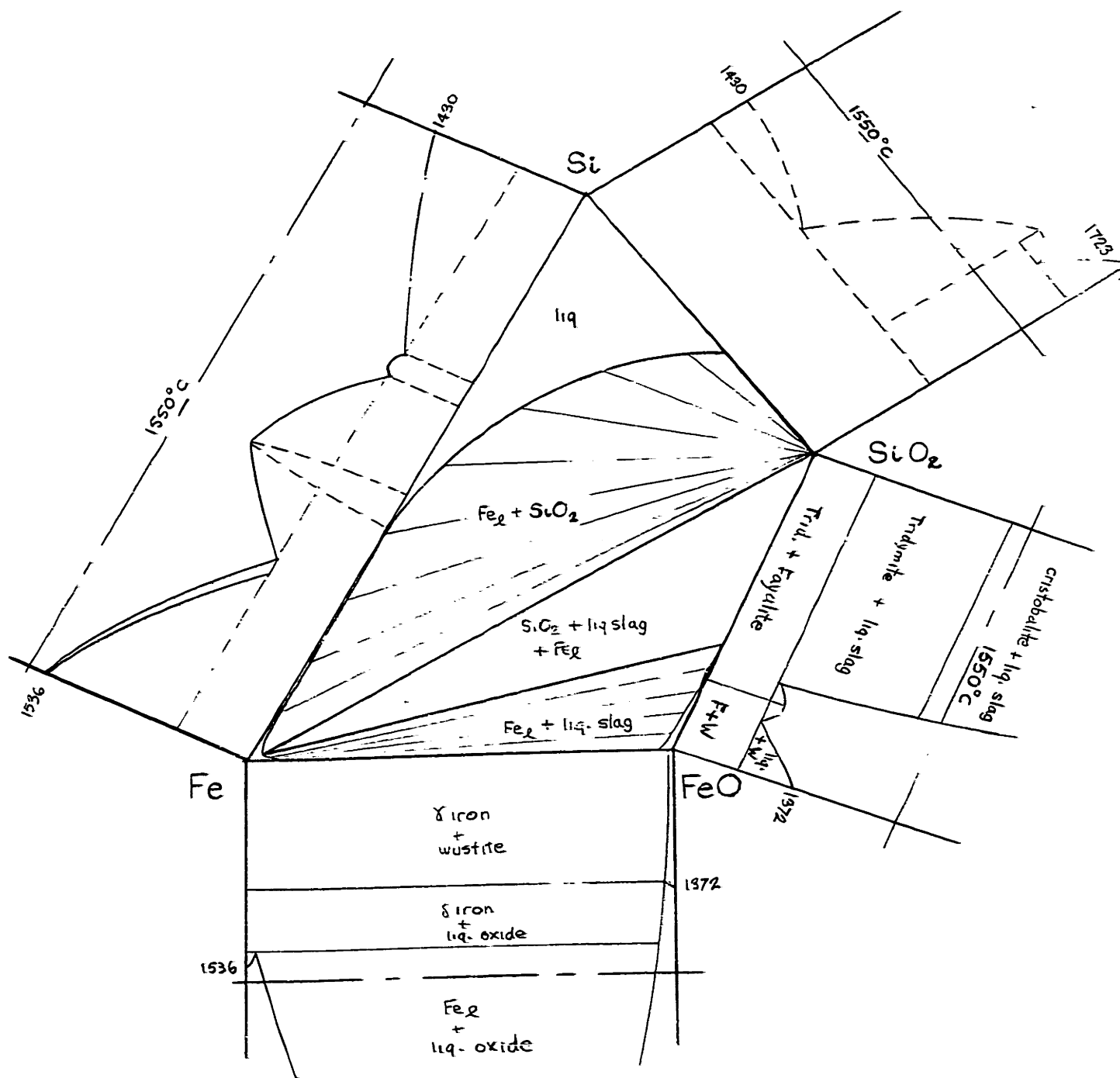


**Figure 2:** Isothermal Section of the Fe-Si-O System - 1550 °C.



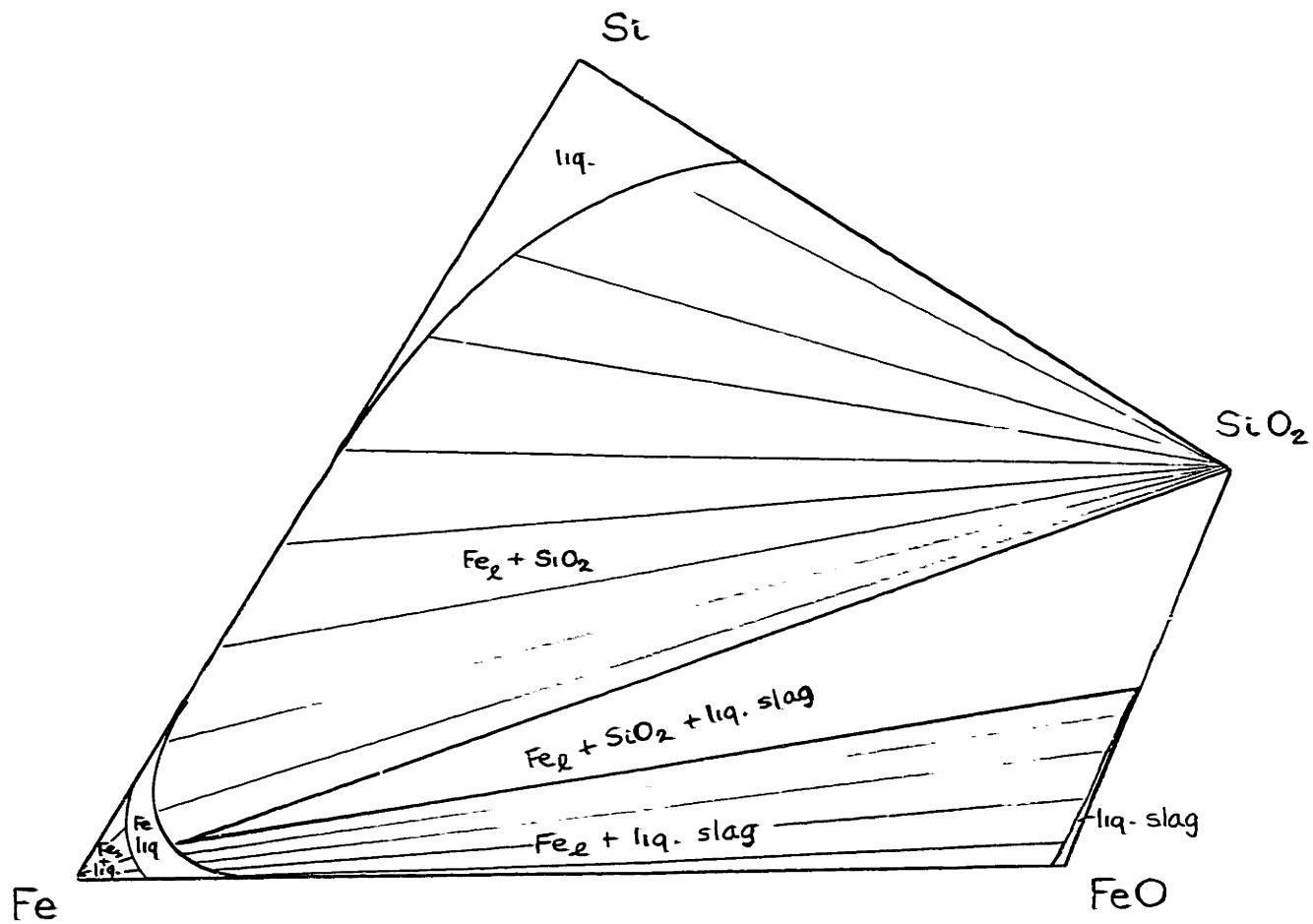


Figure 3: Isothermal Section of the Fe-Si-O System - 1535°C.

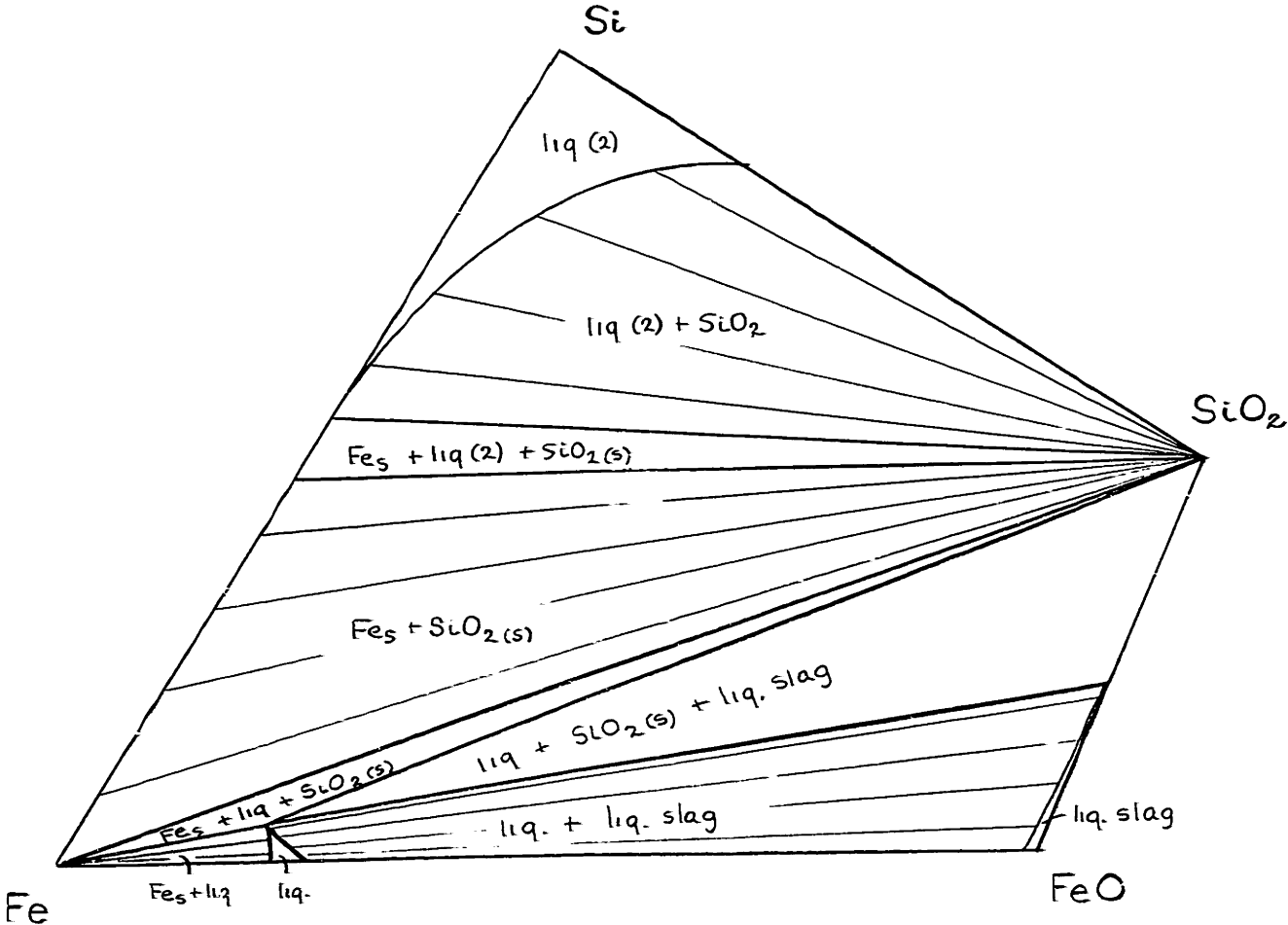


Figure 4: Isothermal Section of the Fe-Si-O System - 1530 °C.

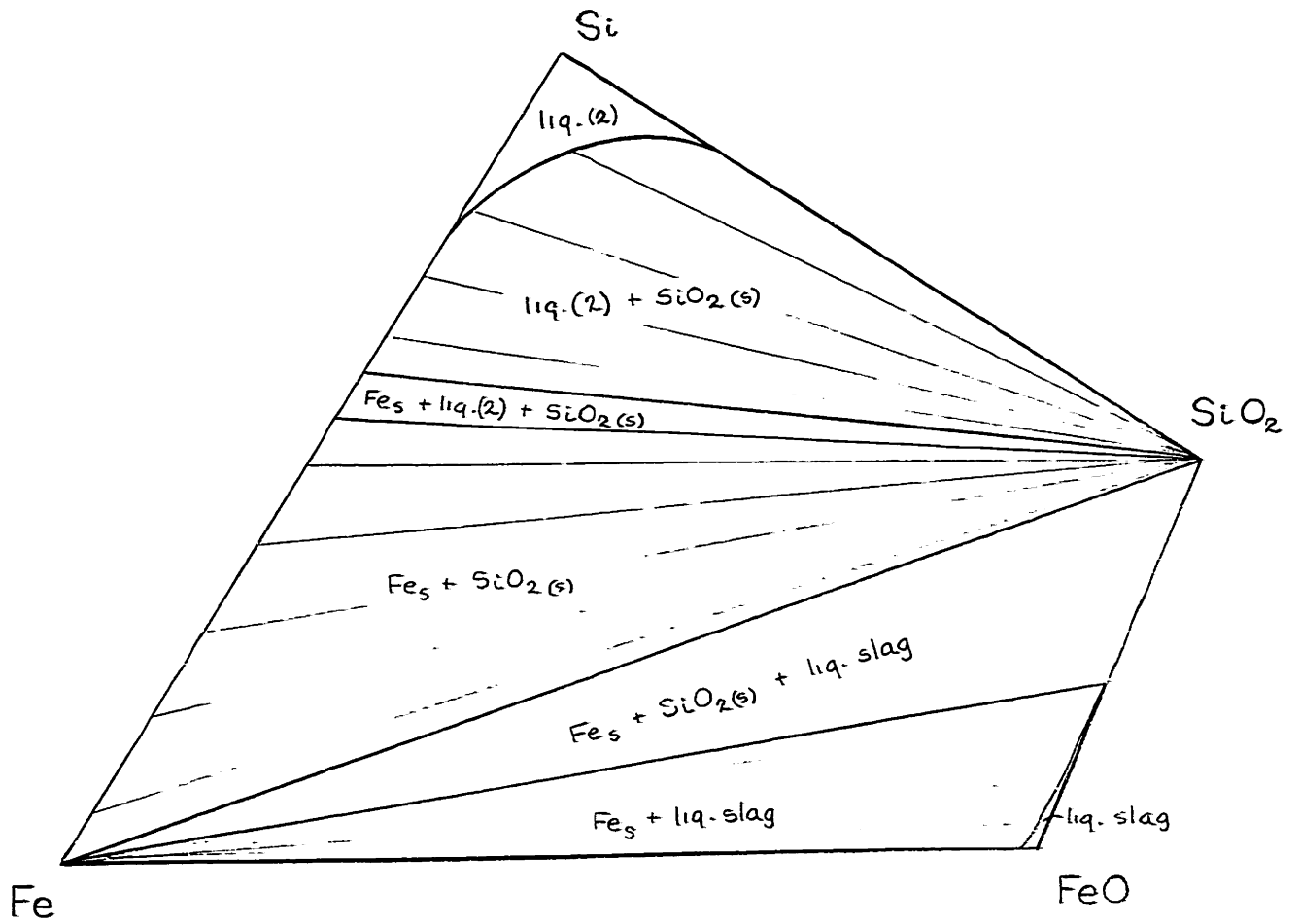


Figure 5: Isothermal Section of the Fe-Si-O System - 1500 °C.

The Iron-Rich Corner

Of special interest in this study is the iron-rich corner of the Fe-Si-O system. As mentioned earlier, considerable equilibrium data exist for this region. The solubility limits of silicon and oxygen in liquid iron for 1650°C, 1550°C and 1535°C are shown in Figure 6.

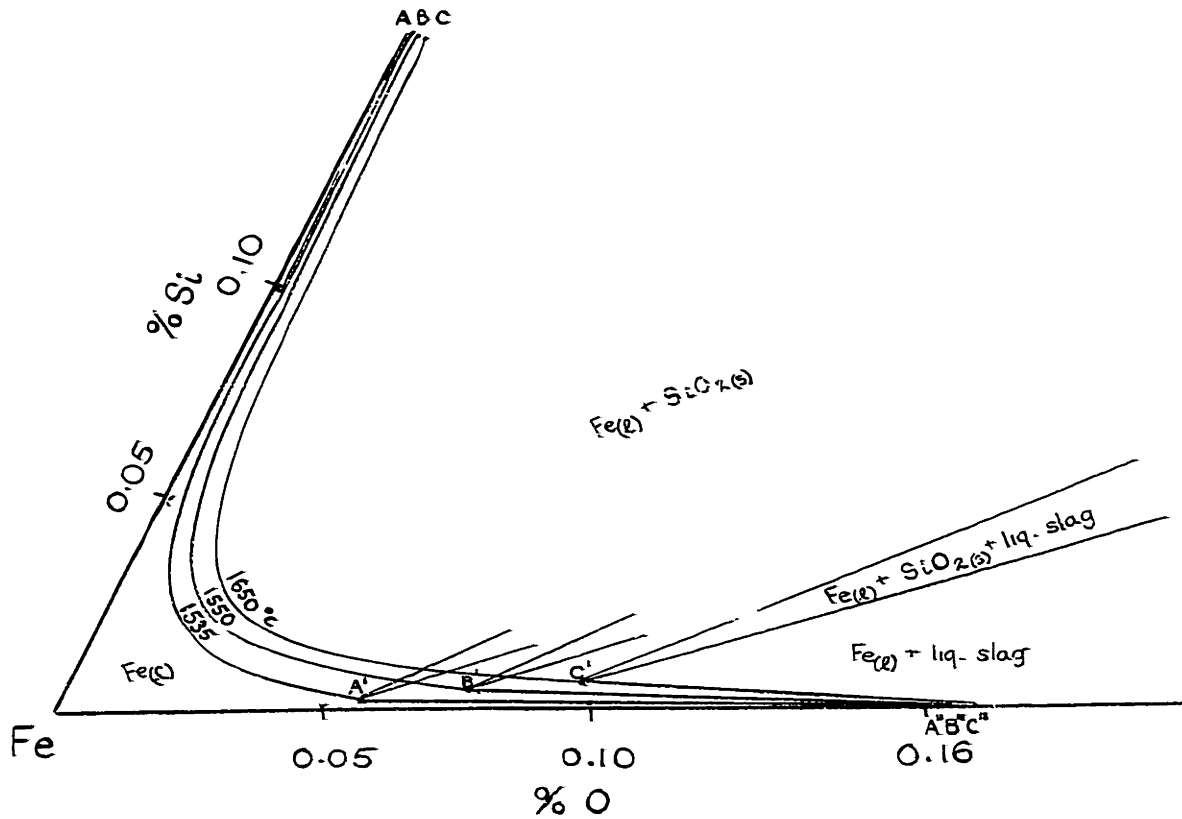
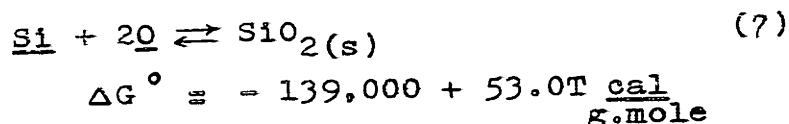
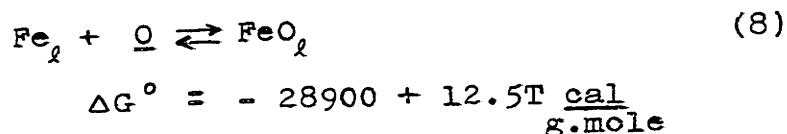


Figure 6: Equilibrium solubility limits for silicon and oxygen in liquid iron.

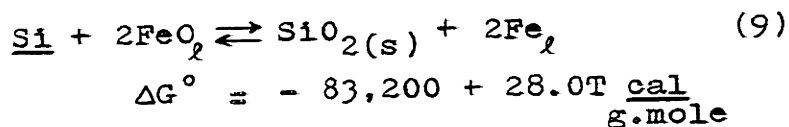
The locations of lines AA', BB' and CC' were calculated from the equilibrium expression<sup>24</sup>,



Points A', B' and C' are invariant points corresponding to three phase equilibrium -- liquid iron-silica-liquid slag. The lines A'A'', B'B'' and C'C'' represent a series of liquid iron compositions in equilibrium with unsaturated liquid FeO-SiO<sub>2</sub> slags. Points A'', B'' and C'' are in the Fe-FeO binary system and are the points of saturation of the liquid iron at the given temperature<sup>25</sup>. With the aid of the following free energy relationship<sup>26</sup>,

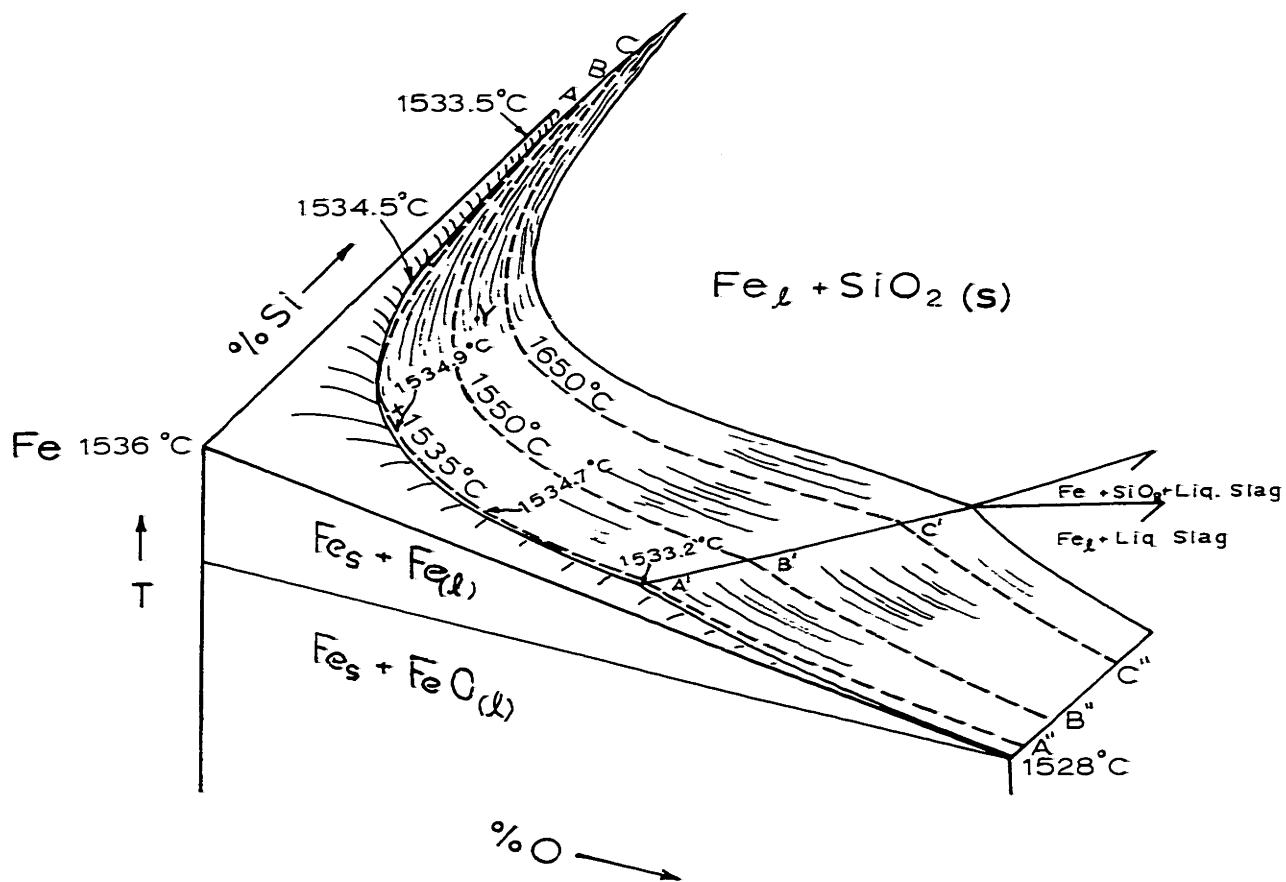


plus equation (1) and a knowledge of FeO and SiO<sub>2</sub> activities in unsaturated slags<sup>27</sup>, lines A'A'', B'B'' and C'C'' were calculated from the expression



The details of this calculation are presented in Appendix A.

Perhaps the best way for one to visualize this rather complex system is to look at a schematic three dimensional representation. This is shown in Figure 7.



Iron Rich Corner of the Fe-Si-O System

FIGURE 7

Lines AA'A", BB'B" and CC'C" are those from Figure 6. There exists in the system a line of intersection between two downward sloping surfaces of saturation - liquid iron with solid iron and liquid iron with silica or liquid iron with liquid slag. This intersection is a line of three phase equilibrium or two-fold saturation - liquid iron with solid iron and silica or liquid iron with solid iron and liquid slag - and forms a sort of "valley" bottom. The position of this line is very close to the silicon and oxygen compositions calculated from equilibrium data for 1535°C. The temperatures were calculated from freezing point lowering considerations, the details of which are shown in Appendix B. Point "X" in Figure 7 is at 0.04 wt% silicon, 0.013 wt% oxygen and 1534.9°C, and is the maximum temperature for the line of two-fold saturation. From this point the "valley" descends towards the Fe-Si binary and towards the Fe-O binary. The significance of point "X" will become apparent in the following section in which the process of solidification is examined.

## B. MODEL I, "BARRIER-FREE" SOLIDIFICATION

Consider a liquid of composition "Y", in Figure 7, at 1600°C somewhere on the surface of saturation in equilibrium with silica. If the liquid is now cooled and equilibrium with the oxide phase is maintained, silica particles will precipitate and grow in the liquid. The composition of the liquid will move down the surface towards the line of two-fold saturation. At the line of two-fold saturation iron begins to solidify. The following analysis traces the course of solidification of five liquids situated at different positions along the line of two-fold saturation.

In this analysis the following assumptions are made:

a. No nucleation barrier exists for the formation of the oxide phases and the oxide phases are at all times in equilibrium with the surrounding liquid.

b. There is negligible diffusion of the solutes in solid iron.

c. The composition of the solutes in the interdendritic liquid is uniform.

d. The oxide particles when precipitated in liquid iron are trapped in the advancing solid-liquid interface and are not pushed ahead.

### 1. Solute rejection during freezing

To determine the amount of silicon and oxygen rejected into the liquid iron for a given fraction of the iron



solidified, plots of liquid composition versus fraction of iron solidified were constructed from the solidification relationship<sup>28</sup>,

$$C_{\ell} = C_0 [1 - f_s]^{(k_0 - 1)} \quad (10)$$

where  $C_{\ell}$  = composition of the liquid

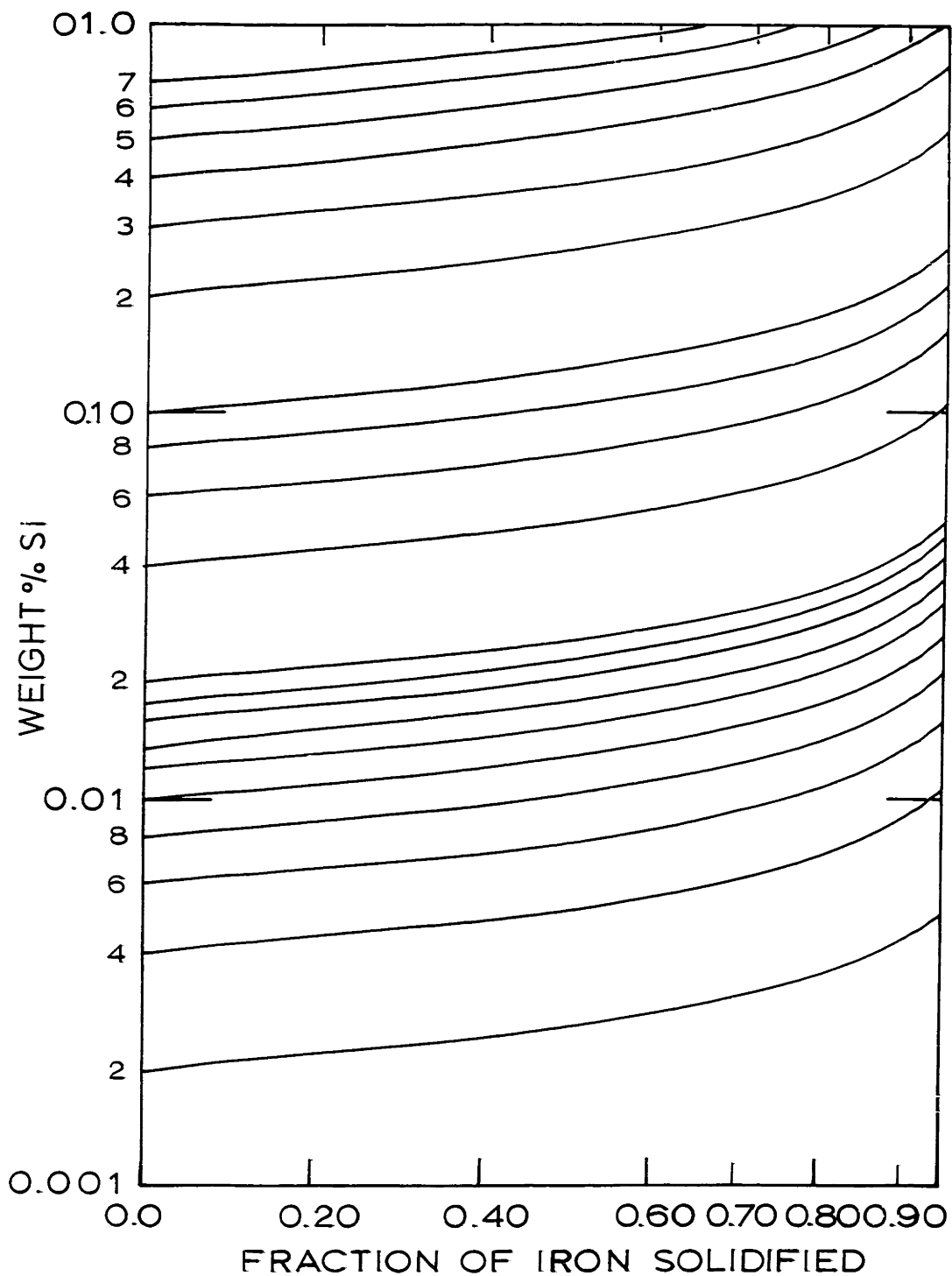
$C_0$  = initial composition of the liquid

$k_0$  = equilibrium distribution for the solute in question and is  $\frac{C_s}{C_{\ell}}$ , where  $C_s$  is the equilibrium concentration of the solute in solid iron

$f_s$  = fraction of the iron solidified

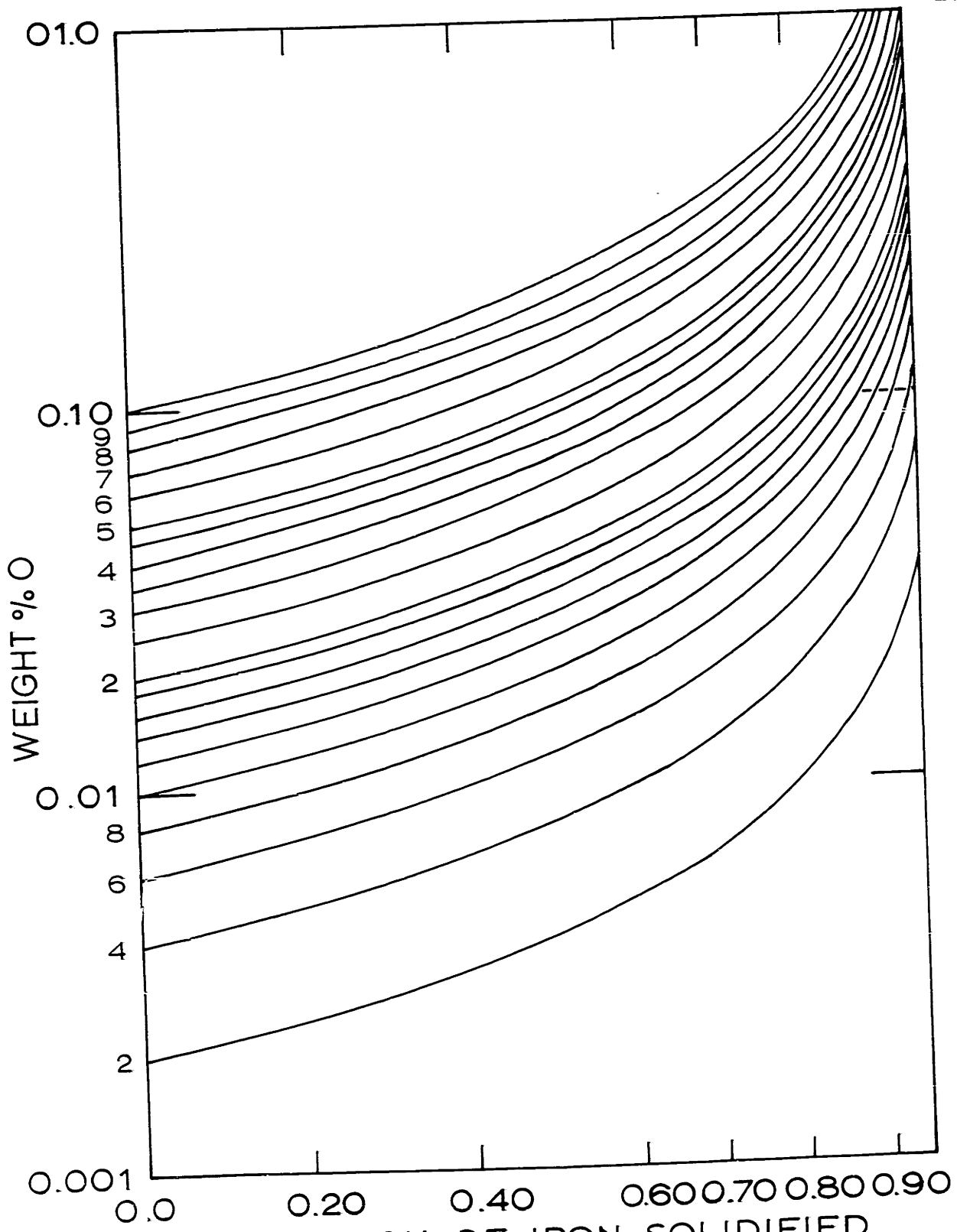
The value of  $k_0$  for silicon was taken to be 0.67<sup>16</sup> whereas  $k_0$  for oxygen was assumed to be zero. Hempworth<sup>29</sup> has measured  $k_0$  for oxygen in iron and proposes a value of 0.059. The results, when calculated using this new value, were not substantially different from those obtained using  $k_0 = 0.0$ . Thus, for reasons of simplification, the later value was used.

Plots of  $f_s$  versus wt%Si and wt%O in liquid iron are shown in Figures 8 and 9.



Weight % Si in Liquid Iron vs. Fraction of Iron Solidified

FIGURE 8



Weight % O in Liquid Iron vs. Fraction of Iron Solidified

FIGURE 9

## 2. Method of calculation

Starting with liquid compositions corresponding to points on the line of two-fold saturation, the process of solidification was followed in which the composition of the remaining liquid was calculated for various fractions of the melt solidified. For each solidification step the composition of the remaining liquid was first picked off from the plots of  $f_s$  versus wt%O and wt%Si assuming no reaction between the rejected solutes. Then the liquid composition was adjusted by removing Si and O as  $\text{SiO}_2$  until the liquid iron-silica equilibrium for  $1535^\circ\text{C}$  was again satisfied. The process was repeated for the next step of solidification only now the "initial" liquid composition was the equilibrium value determined from the previous step. In this manner the liquid composition changes and the amounts of  $\text{SiO}_2$  precipitated as a function of iron solidified were calculated. The results for five different liquids are shown in Tables 1-5.

## 3. Metallographic interpretation

Below each of the tables is a diagram depicting a metallographic cross-section of the solid iron showing the distributions, and compositions of inclusions precipitated during "Barrier Free" solidification (Figures 10-14). Each figure represents a single unit or dendrite of iron. As mentioned earlier it is assumed that particles formed during solidification are not pushed ahead of the advancing solid iron-liquid interface but become trapped in the solid iron.

Thus, their position in the metallographic cross-section is related to the fraction of iron solidified at the time of their formation. For instance, if an oxide particle is formed when 50 percent of the iron is solid, then the particle, in the solid section, appears halfway between the dendrite center line and the dendrite edge.

Fraction of Metal Solidified	Composition of Liquid If No Reactions		Composition of Equilibrium Liquid		Cum. Fraction of Original O ppted As SiO <sub>2</sub>
	f <sub>s</sub>	wt%Si	wt%O	wt%Sieq	
0.00	0.200	0.0059	0.200	0.0059	0.000
0.20	0.220	0.0071	0.219	0.0054	0.240
0.40	0.250	0.0072	0.248	0.0051	0.490
0.60	0.290	0.0074	0.288	0.0048	0.680
0.80	0.370	0.0100	0.365	0.0042	0.855
0.90	0.460	0.0084	0.456	0.0038	0.935
0.95	0.580	0.0076	0.576	0.0034	0.991
0.975	0.730	0.0066	0.727	0.0030	0.995

Table 1: Liquid A; Initial composition Si=0.20%, O=0.0059%

Conclusion: During solidification the composition of the equilibrium interdendritic liquid moves towards higher silicon. 100% of the original oxygen precipitates as SiO<sub>2</sub>.

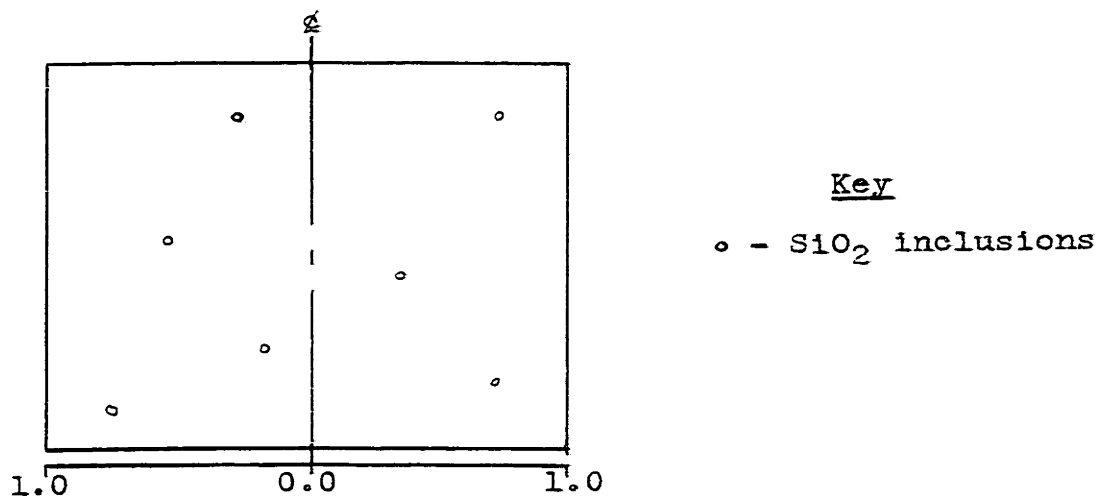


Figure 10: Resulting Micrograph for Liquid A.

Fraction of Metal Solidified $f_s$	Composition of Liquid If No Reactions		Composition of Equilibrium Liquid		Cum. Fraction of Original O ppted As $SiO_2$
	wt%Si	wt%O	wt%Sieq	wt%Oeq	
0.00	0.100	0.008	0.100	0.008	0.000
0.20	0.110	0.010	0.109	0.008	0.200
0.40	0.120	0.0105	0.117	0.0071	0.454
0.60	0.130	0.011	0.127	0.0067	0.665
0.80	0.160	0.014	0.154	0.0063	0.845
0.90	0.185	0.013	0.179	0.0060	0.925
0.95	0.220	0.012	0.215	0.0054	0.968
0.975	0.280	0.011	0.275	0.0048	0.980

Table 2: Liquid B; Initial composition Si=0.10%, O=0.008%

Conclusion: Composition of the remaining liquid moves down the Fe-Si valley towards high Si. 100% of the precipitate is  $SiO_2$ .

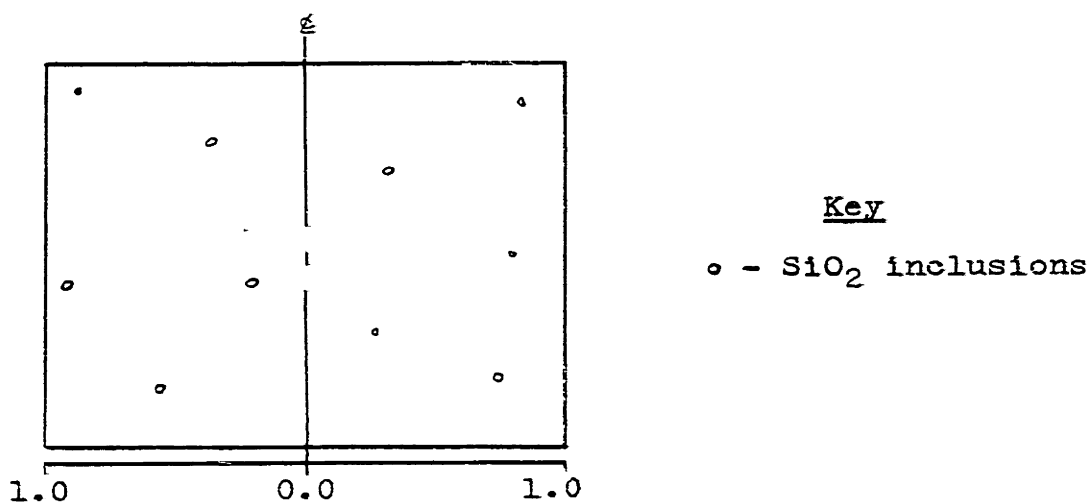


Figure 11: Resulting Micrograph for Liquid B.

Fraction of Metal Solidified	Composition of Liquid If No Reactions		Composition of Equilibrium Liquid		Cum. Fraction of Original $O$ pptd As $SiO_2$
	wt%Si	wt%O	wt%Sieq	wt%Oeq	
0.00	0.040	0.013	0.040	0.0130	0.000
0.20	0.044	0.016	0.040	0.0130	0.200
0.40	0.045	0.017	0.041	0.0124	0.435
0.60	0.048	0.018	0.043	0.0123	0.650
0.80	0.057	0.026	0.045	0.0120	0.815
0.90	0.0574	0.026	0.0451	0.0119	0.908
0.95	0.0575	0.026	0.0452	0.0118	0.954
0.975	0.0575	0.026	0.0453	0.0117	0.977

Table 3: Liquid C; Initial composition Si=0.040%, O=0.013%

Conclusion: The composition of the equilibrium interdendritic liquid changes very little during the solidification process. 100% of the original oxygen precipitates as  $SiO_2$ .

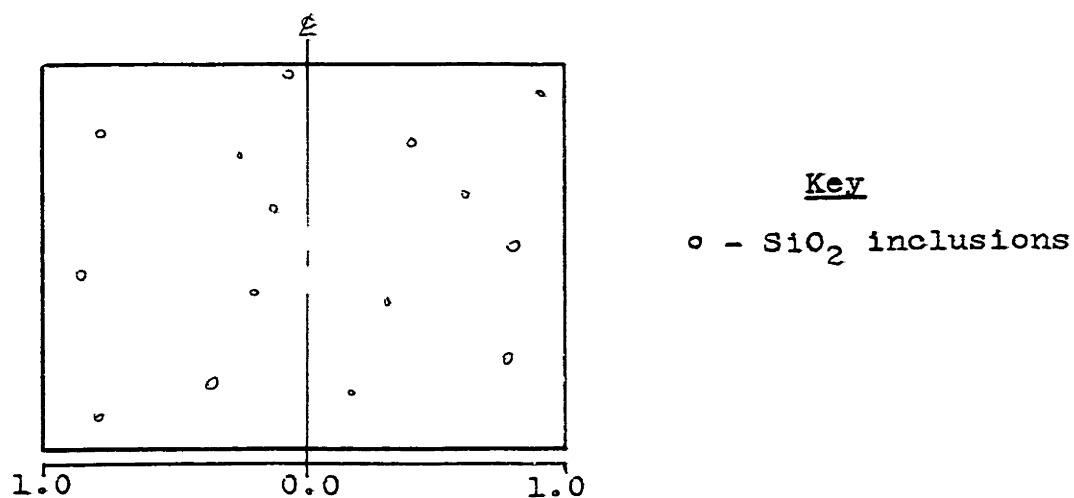


Figure 12: Resulting Micrograph for Liquid C.



Fraction of Metal Solidified	Composition of Liquid If No Reactions		Composition of Equilibrium Liquid		Cum. Fraction of Original O pptd As SiO <sub>2</sub>
	wt%Si	wt%O	wt%Sieq	wt%Oeq	
0.00	0.0100	0.025	0.0100	0.0250	0.000
0.20	0.0110	0.031	0.0085	0.0282	0.130
0.40	0.0094	0.036	0.0060	0.0320	0.244
0.60	0.0069	0.047	0.0030	0.0430	0.316
0.70	0.0035	0.056	0.0019	0.0551	0.350

Table 4: Liquid D; Initial composition Si=0.010%, O=0.025%

Conclusion: 35% of the original oxygen is precipitated as SiO<sub>2</sub>. During solidification the equilibrium dendritic liquid increases in oxygen achieving silica saturation when 71% of the iron is solid. A small amount of mixed silicates precipitate at silica saturation with solidification now taking place in the Fe-O binary system. The balance of the oxygen precipitates as an Fe-FeO eutectic when the liquid contains 0.16% O and iron is 88% solidified.

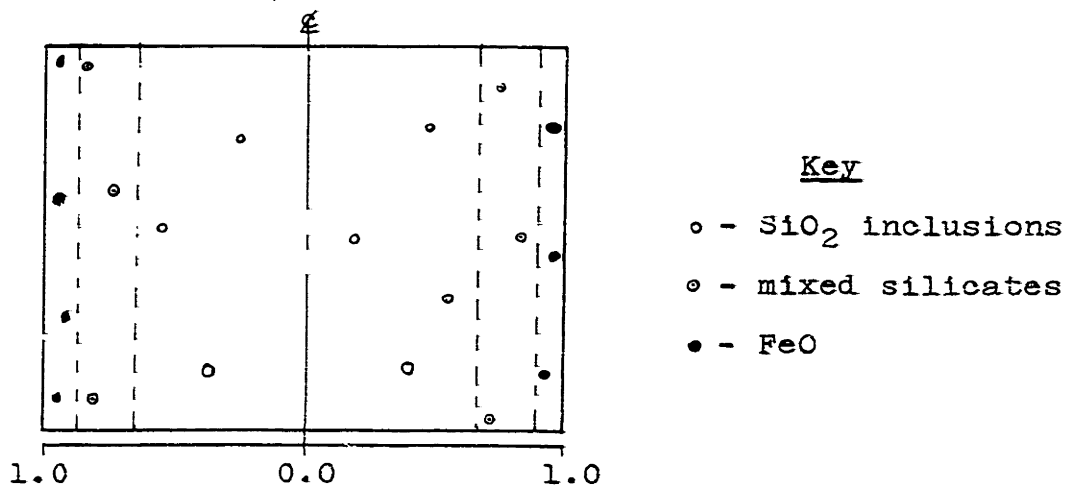


Figure 13: Resulting Micrograph for Liquid D.

Fraction of Metal Solidified	Composition of Liquid If No Reactions		Composition of Equilibrium Liquid		Cum. Fraction of Original O ppted As SiO <sub>2</sub>
	wt%Si	wt%O	wt%Sieq	wt%Oeq	
0.00	0.0015	0.061	0.0	0.061	trace
0.20	0.0000	0.076	0.0	0.076	"
0.40	0.0000	0.101	0.0	0.101	"
0.60	0.0000	0.160	0.0	0.160	"

Table 5: Liquid E; Initial composition Si=0.0015%, O=0.061%  
 Conclusion: Solidification is primarily in the Fe-O binary system. Minute amounts of mixed silicates are formed early in the solidification process. When the iron is 60% solidified the balance of the oxygen precipitated as an Fe-FeO eutectic. The composition of the oxide end product is ~100%FeO.

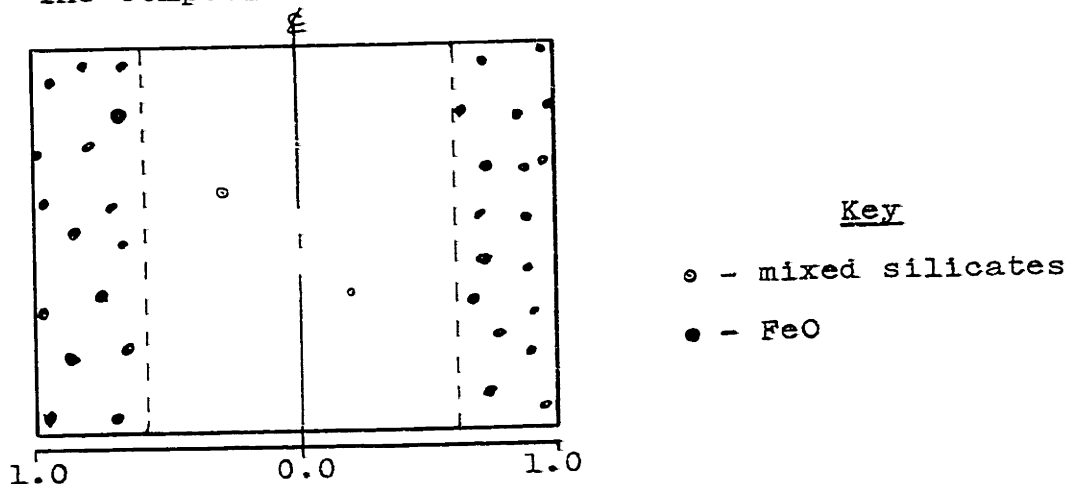
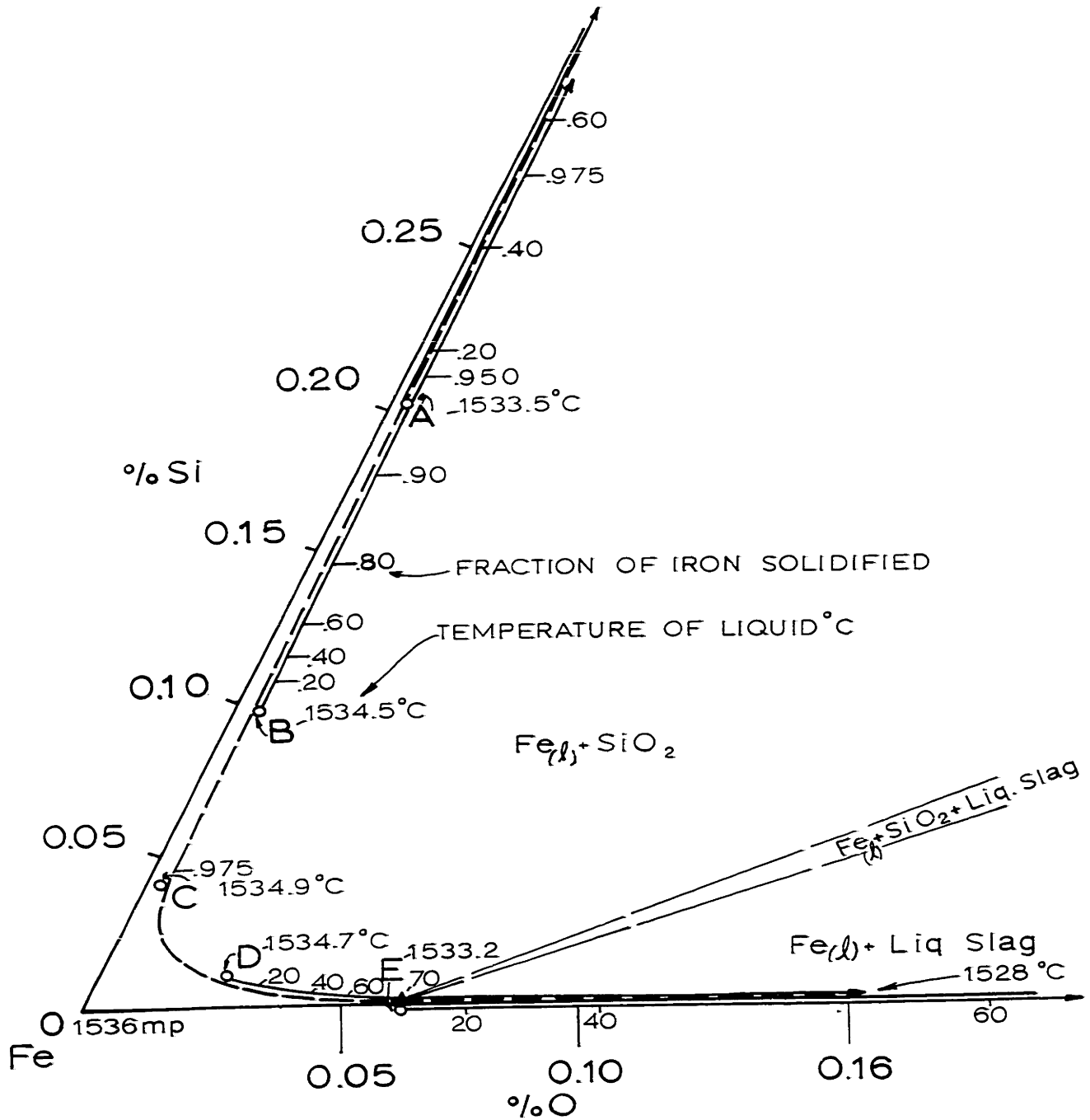


Figure 14: Resulting Micrograph for Liquid E.

Figure 15 shows the liquid composition changes during "Barrier-Free" solidification as calculated above. The open circles represent the initial liquid compositions. The arrows indicate the direction of the liquid composition changes and the fractions represent the amount of iron solidified.



Liquid Composition Changes During  
Barrier Free Solidification  
MODEL I

FIGURE 15

The results of "Barrier-Free" solidification of iron melts situated along the line of two-fold saturation in the Fe-Si-O system may be summarized as follows:

a. Initial silicon content of liquid above 0.04 Wt%;

All oxygen will precipitate as  $\text{SiO}_2$ . The inclusions will appear as glassy  $\text{SiO}_2$  spheres situated at random across iron dendrites. The multiplicity of inclusions will increase with decreasing initial silicon concentration.

b. Initial silicon content of liquid less than 0.04 Wt% but greater than 0.0015 Wt%;

Many inclusions will appear as  $\text{SiO}_2$  particles situated at random in the dendrites. Closer to the dendrite boundaries a narrow zone of mixed silicates will appear. The balance of the oxygen will precipitate as an Fe-FeO eutectic at the periphery of the dendrite.

c. Initial silicon content of liquid at silica saturation,  $S_1 = 0.0015$  Wt%;

All oxygen will precipitate in the form of an Fe-FeO eutectic appearing when the iron is 60 percent solidified.

### C. MODEL II, "BARRIER" SOLIDIFICATION

The solidification of the liquids studied in the previous section will now be followed according to the so-called "Barrier" solidification. In this analysis the following assumptions are made:

a. The liquids contain no nuclei or substrates upon which the oxide phases may nucleate and grow. During the solidification of iron the interdendritic liquid is enriched with the rejected solutes until the "barrier" for homogeneous nucleation is crossed. At this point an oxide phase precipitates.

b. For purposes of comparison it is assumed that nucleation occurs at those supersaturations calculated by Turpin and Elliott for which  $\sigma_{Fe_l - FeO_l} = 250 \text{ ergs/cm}^2$  and  $\sigma_{Fe_l - SiO_2} = 1300 \text{ ergs/cm}^2$ .

c. There is negligible diffusion of the solutes in solid iron.

d. The concentration of each solute in the interdendritic liquid is uniform.

e. The oxide particles when precipitated in the liquid iron are not displaced by the advancing solid - liquid interface.

The concentrations of silicon and oxygen in the liquid as a function of the fraction of iron solidified were obtained, as before, from Figures 8 and 9.

The results of these calculations are shown in Tables 6 - 10. The critical supersaturations are identified by asterisks. Also shown is the temperature of the liquid as calculated from freezing point lowering considerations. Figures 16 - 20 portray the metallographic interpretations.

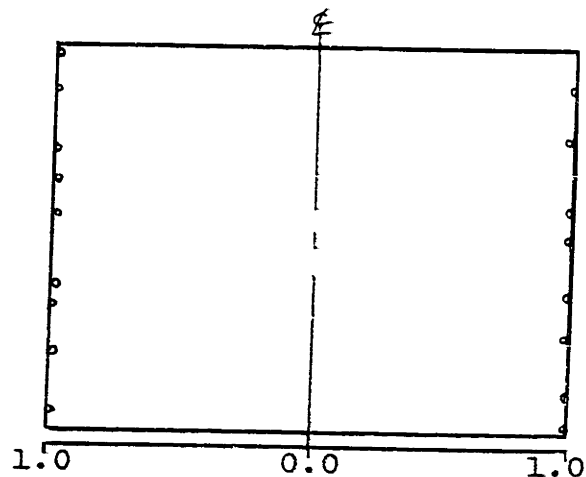
Fraction of Metal Solidified	Composition of Remaining Liquid		Liquid Temperature	Supercooling*
	wt%Si	wt%O	T (°C)	T <sub>eq</sub> - T (°C)
0.00	0.200	0.0059	1533.4	0.0
0.20	0.220	0.0071	1533.1	0.3
0.40	0.240	0.0100	1532.7	0.7
0.60	0.280	0.015	1531.9	1.5
0.80	0.350	0.029	1531.3	2.1
0.90	0.430	0.058	1527.5	5.9
0.95	0.540	0.116	1523.0	10.4
0.98**	0.650	0.200	1518.1	15.3

Table 6: Liquid A; Initial composition Si=0.20%, O=0.0059%

Conclusion: The inclusions are 100% SiO<sub>2</sub> appearing in the last 2% of the liquid to solidify.

\* Relative to the formation of SiO<sub>2</sub>

\*\* Nucleation



Key  
o - SiO<sub>2</sub> inclusions

Figure 16: Resulting Metallograph for Liquid A.

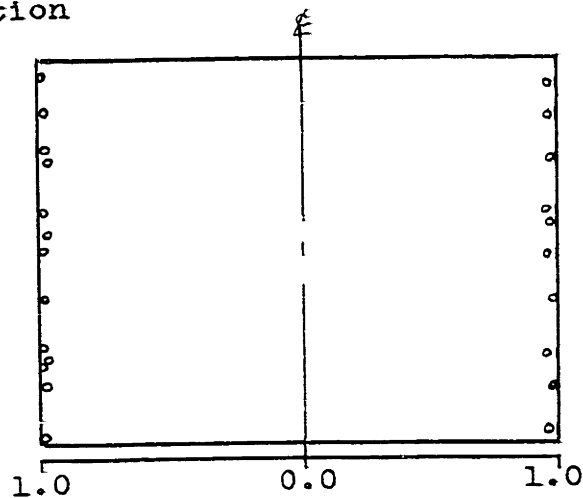
Fraction of Metal Solidified	Composition of Remaining Liquid		Liquid Temperature	Supercooling*
	$f_s$	wt%Si	wt%O	T (°C)
0.00	0.100	0.008	1534.5	0.0
0.20	0.110	0.010	1534.3	0.2
0.40	0.120	0.013	1534.0	0.5
0.60	0.135	0.020	1533.5	1.0
0.80	0.175	0.040	1532.0	2.5
0.90	0.220	0.080	1529.5	4.0
0.95	0.270	0.160	1525.1	9.4
0.97**	0.320	0.290	1517.6	16.9

Table 7: Liquid B; Initial composition Si=0.10%, O=0.008%

Conclusion: The inclusions are 100% SiO<sub>2</sub> appearing in the last 3% of the metal to solidify.

\* Relative to the formation of SiO<sub>2</sub>

\*\* Nucleation



Key

o - SiO<sub>2</sub> inclusions

Figure 17: Resulting Micrograph for Liquid B.



Fraction of Metal Solidified	Composition of Remaining Liquid		Liquid Temperature	Supercooling*
	wt%Si	wt%O	T (°C)	Teq - T (°C)
0.00	0.040	0.013	1534.9	0.0
0.20	0.044	0.016	1534.7	0.2
0.40	0.048	0.022	1534.3	0.6
0.60	0.054	0.035	1533.7	1.2
0.80	0.060	0.065	1532.1	2.8
0.90	0.086	0.130	1528.6	6.3
0.95	0.110	0.260	1518.8	13.1
0.96**	0.120	0.310	1519.2	15.7

Table 8: Liquid C; Initial composition Si=0.040%, O=0.0130%

Conclusion: Inclusions appear in the last 4% of the liquid to solidify. 44% of the total oxygen will appear as SiO<sub>2</sub>, 56% as FeO.

\* Relative to the formation of SiO<sub>2</sub>, \*\*Nucleation

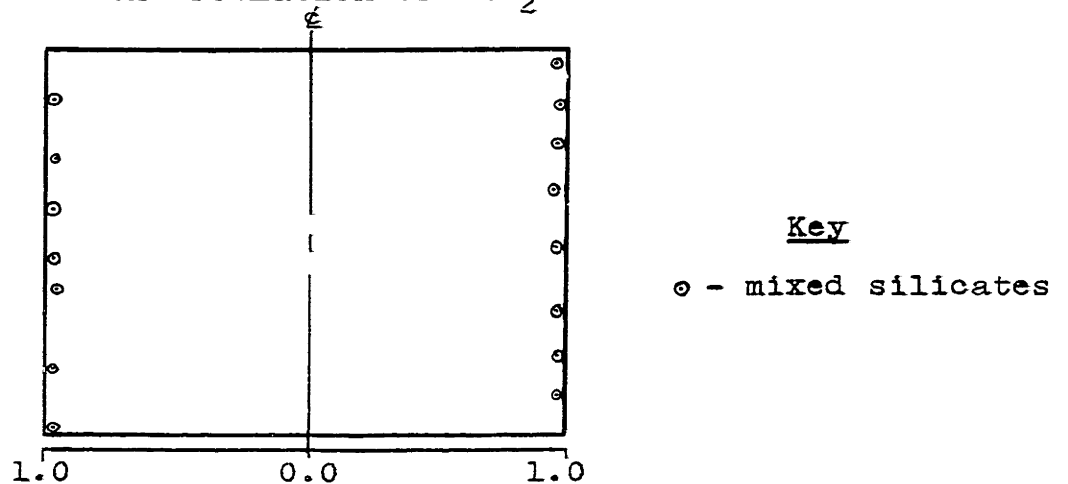


Figure 18: Resulting Micrograph for Liquid C.

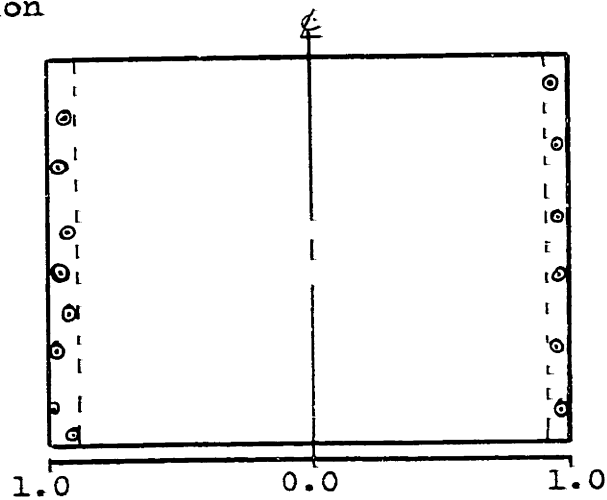
Fraction of Metal Solidified	Composition of Remaining Liquid		Liquid Temperature	Supercooling*
	wt%Si	wt%O		
$f_s$			T (°C)	$T_{eq} - T$ (°C)
0.00	0.010	0.025	1534.7	0.0
0.20	0.011	0.031	1534.3	0.4
0.40	0.012	0.042	1533.8	0.9
0.60	0.014	0.063	1532.8	1.9
0.80	0.017	0.125	1530.1	4.6
0.90	0.021	0.250	1523.3	11.4
0.91**	0.022	0.310	1520.3	14.4

Table 9: Liquid D; Initial composition Si=0.010%, O=0.025%

Conclusion: Inclusions will appear in the last 9% of the liquid to solidify. 8% of the original oxygen will appear as  $SiO_2$ , 92% as FeO.

\*Relative to the formation of  $SiO_2$

\*\*Nucleation



Key  
 ⊙ - mixed silicates

Figure 19: Resulting Micrograph for Liquid D.

Fraction of Metal Solidified	Composition of Remaining Liquid		Liquid Temperature	Supercooling*
	$f_s$	wt%Si	wt%O	T (°C)
0.00	0.0015	0.061	1533.0	0.0
0.20	0.0016	0.076	1532.2	0.8
0.40	0.0018	0.101	1531.0	2.0
0.60	0.0020	0.160	1528.0	5.0
0.80**	0.0026	0.310	1520.7	12.3

Table 10: Liquid E; Initial composition Si=0.0015%, O=0.061%

Conclusion: Inclusions will appear as an Fe-FeO eutectic in the last 20T of the liquid to solidify. 100% of the original oxygen will appear as FeO.

\* Relative to the formation of  $SiO_2$

\*\* Nucleation

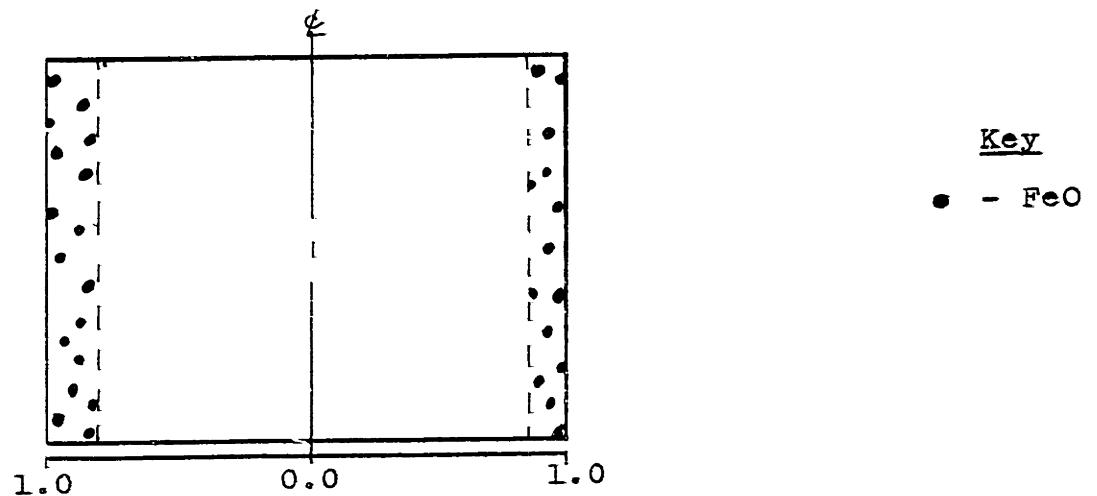


Figure 20: Resulting Micrograph for Liquid E.

The results of this analysis are shown in Figure 21.

In this figure the dashed lines indicate the composition paths followed by the interdendritic liquid during the course of solidification. The numbers above the lines indicate the temperature of the liquid at this composition and those below the line represent the fraction of the iron solidified. Also shown in the ternary system are the nucleation lines for  $\text{SiO}_2$  and  $\text{FeO}$  as calculated by Turpin. If, in fact, the oxide phases did precipitate at supersaturations of this order they would by this analysis appear in the last fractions of the liquid to solidify as indicated on the diagram.

A summary of the results expected from "Barrier" solidification of the five melts is presented below.

a. Initial silicon content of the liquid above 0.10 Wt%;

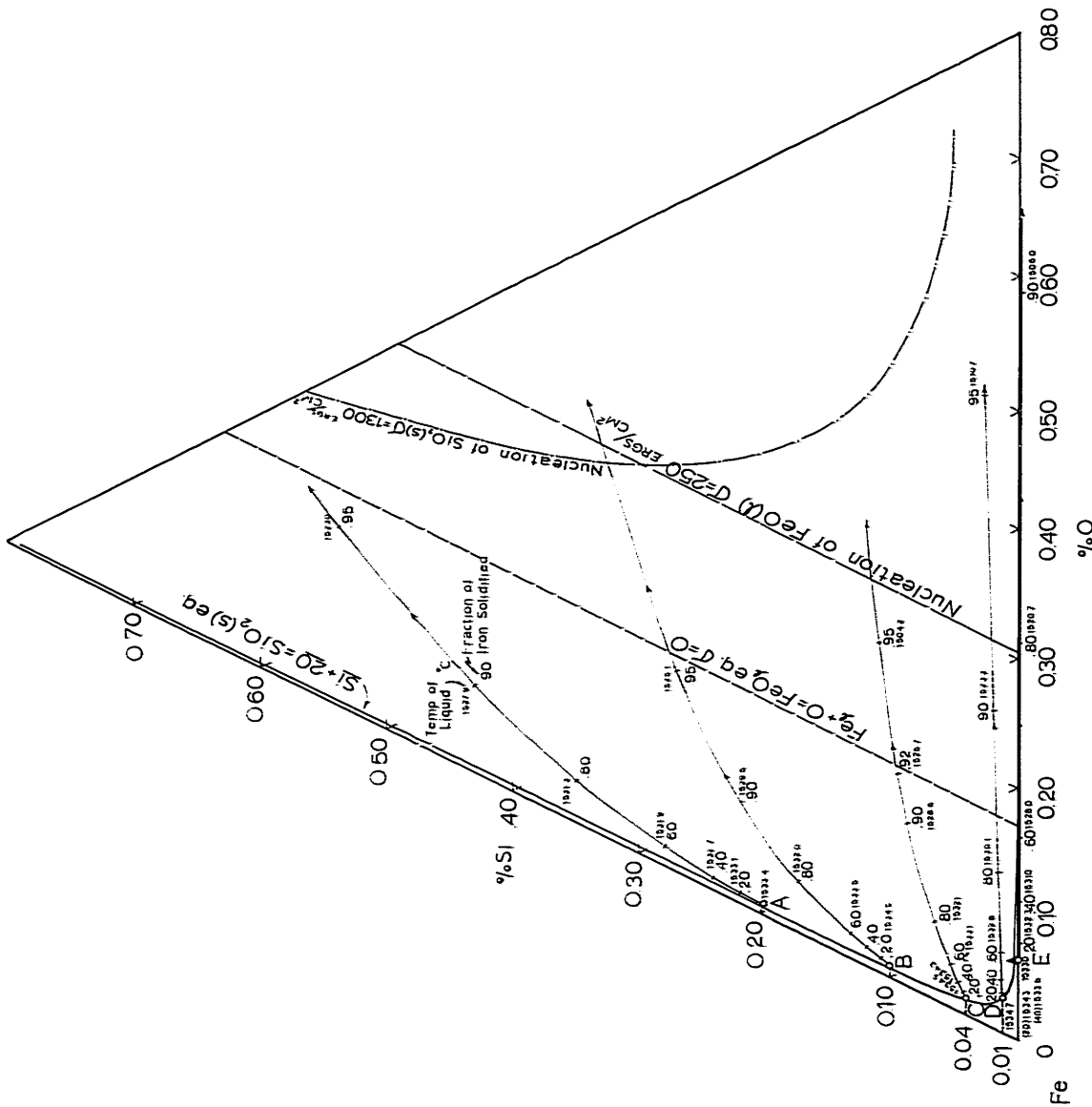
The inclusions will be 100 percent  $\text{SiO}_2$  appearing at the dendrite boundaries.

b. Initial silicon content of the liquid below 0.10 Wt% and above 0.010 Wt%;

The particles will appear at the dendrite boundaries and will be mixed silicates approaching almost pure  $\text{FeO}$  at 0.010 Wt% Si.

c. Below 0.010 Wt% Si initial content;

The inclusions will be virtually pure  $\text{FeO}$  appearing as a eutectic when 80% of the iron has solidified.



Liquid Composition Changes During Barrier Solidification  
 MODEL II  
 FIGURE 21

D. MODEL III, "BARRIER-FREE" SOLIDIFICATION WITH MOBILE PARTICLES

A third mechanism for the formation of inclusions has been considered. Oxide particles could precipitate early in the solidification process, as described in the Barrier-Free model, and be pushed ahead by advancing solid iron - liquid interface. If this were the case, then all particles would appear at the primary dendrite boundaries.

The following evidence would indicate that this does not occur. Chalmers and Uhlmann<sup>30</sup> have performed solidification experiments with orthophenyl liquid containing a suspension of MgO particles. They determined that there exists a critical velocity of the solid - liquid interface below which particles are pushed ahead. This velocity is extremely low and is of the order of  $0.5 \mu/\text{sec}$ , well below that normally encountered in metal solidification. They also found that this critical speed is independent of particle size. For these reasons, plus further evidence to be cited in the text of the thesis, it is assumed that a model based on the hypothesis that particles are pushed ahead by the solid - liquid interface could be rejected.

#### IV. APPARATUS, EXPERIMENTAL MATERIALS AND PROCEDURE

##### A. DESCRIPTION OF APPARATUS:

##### 1. Gas Purification

A flow diagram of the gas purification system is shown in Figure 22.

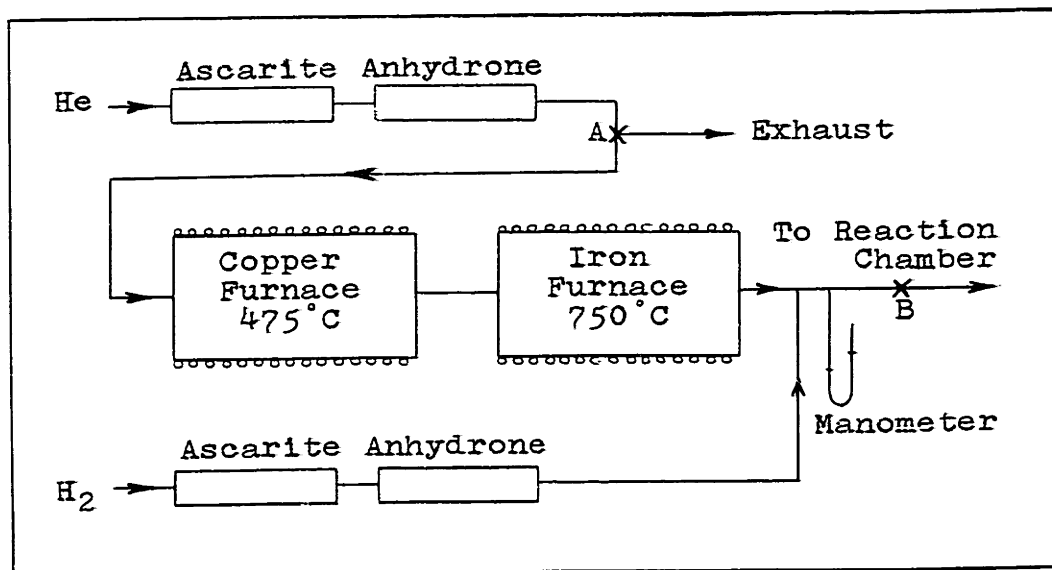


Figure 22: Gas Purification System

Helium supplied by the Airco Company was passed through copper and iron furnaces arranged in series to remove trace amounts of oxygen before entry into the furnace chamber.

Hydrogen, also supplied by Airco, and used during melt-down and for quenching, was passed through columns of ascarite and anhydron before entering the furnace.

The copper and iron furnaces were periodically regenerated with hydrogen. This was effected by closing valve "B" in Figure 22 and turning the two-way stop-cock "A" to the exhaust position thus forcing the hydrogen through the furnaces.

## 2. Experimental Apparatus

A detailed drawing of the reaction chamber is shown in Figure 23. The melts weighing thirty grams were contained in fused silica crucibles supplied by Synchor Products Ltd. of Malden, Massachusetts. The crucibles were 1 inch in diameter,  $3/4$  inch high and had a wall thickness of  $1/8$  inch.

The crucibles were set on an alumina stand made by the Ceramics Laboratory at the Massachusetts Institute of Technology. The stand was built in two separate pieces to avoid cracking during rapid quenching. An alundum tube set atop a section of stainless steel tube supported the assembly. An "O-ring" tightened upon the stainless tube in the lower end of the furnace and kept the system gas tight.

An aluminum bracket, which was screwed to the bottom of the tube, contained a miniature radiometric pyrometer. This pyrometer sighted on the bottom of the crucible through an 18 inch long,  $1/8$  inch diameter sapphire rod that served as a light guide. The hot end of the rod was protected against corrosion by a molybdenum cap.



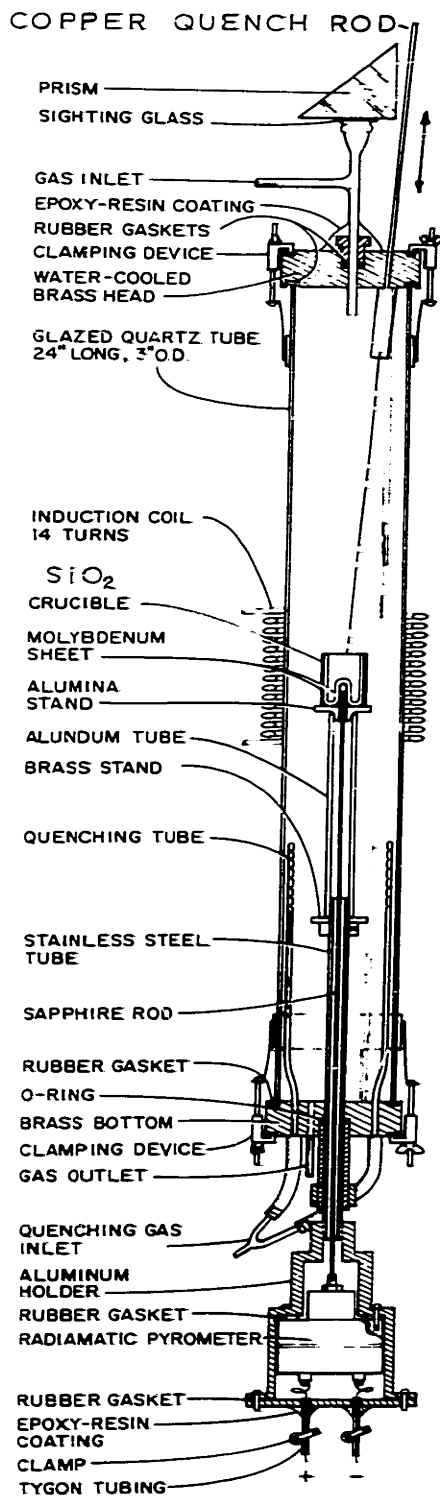


FIGURE - FURNACE ARRANGEMENT

FIGURE 23

The whole assembly was arranged so that at the end of a run, the specimen could be lowered in front of gas vents and quenched in a stream of hydrogen. This technique was developed by Gokcen and Chipman<sup>31</sup>.

For those experiments in which faster solidification rates were desired, a cold copper plug was inserted into the melt. The plug was 3 inches long and 3/8 inch in diameter and was fastened to the end of a long 1/4 inch diameter copper rod extending outside of the furnace (see Figure 23). The copper rod rested in a greased guide clamp and extended through a gas tight seal into the top of the furnace. During a run the copper rod was in its "high" position so that the copper plug touched the water-cooled brass head of the furnace. At the time of quench, the rod was rapidly lowered to a position just above the induction coils, its direction being guided by clamps. The power to the coils was then turned off and the plug plunged quickly into the melt.

#### B. MATERIALS

The melts were prepared from electrolytic iron supplied by the Glidden Company of Johnstown, Pennsylvania. A lot analysis is shown in Appendix E. Silicon additions were in the form of an iron-silicon alloy (32.8% Si by weight).

#### C. EXPERIMENTAL PROCEDURE

Thirty grams of electrolytic iron, in the form of small pieces, and the desired amount of iron-silicon alloy

were placed in a fused silica crucible and inserted in the induction furnace.

The system was checked for leaks by sealing the system, applying a positive pressure of helium and watching for any pressure drop by means of a manometer. If, after ten minutes, there was no drop in pressure, the furnace exit stopcock was opened and the helium flushed through the furnace for a period of two to three hours before melt-down.

During melting a slight flow of hydrogen was maintained to keep the silicon loss at a minimum and to ensure a clean surface on the melted iron.

After melt down, the temperature of the melt was adjusted to the desired value by manipulating the power to the coils. The melt was held at this temperature under a helium atmosphere for one hour. Temperature measurements were taken periodically with an optical pyrometer with an accuracy of  $\pm 5^{\circ}\text{C}$ . Continuous temperature measurements were also made on a Honeywell strip recorder coupled to the total radiation pyrometer.

After equilibration the melt was quenched according to one or other of the quench techniques described in the section on apparatus.

The ingot was removed from the crucible and sectioned for analysis and metallographic examination. Figure 24 portrays a plan of a sectioned ingot indicating the portions of the ingot allotted to specific analyses.

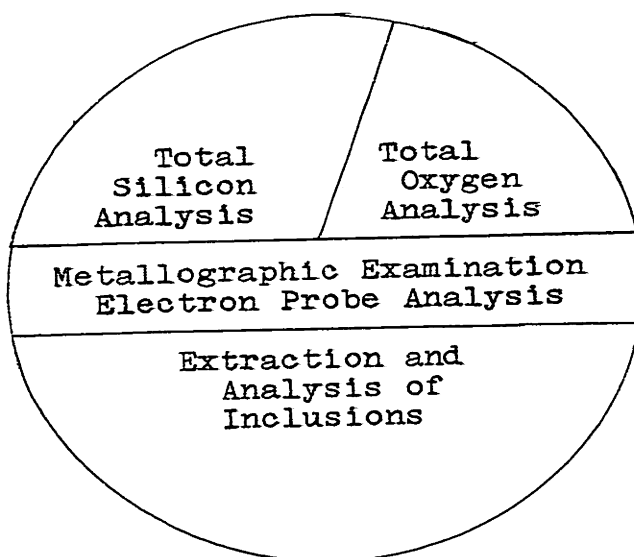


Figure 24: Plan Section of an Ingot Showing Allocations of Portions for Analysis

A slice through the center of the ingot was mounted, polished and examined optically both in ordinary and polarized light. In some cases electron probe studies were performed on mechanically polished sections. Two portions on the ingot, their sizes depending on the anticipated concentrations of the elements in question, were analyzed for total silicon by standard gravimetric procedures and for total oxygen by vacuum fusion. The remainder of the ingot was dissolved in a medium that did not attack the oxide phases thus enabling the identification of the inclusions by chemical analysis, X-Ray and electron diffraction. The details of the extraction process are described in Appendix C.

## V. RESULTS

Three series of experiments were performed. They are classified as follows:

Series Ia; Iron melts containing 0.0 to 0.70 Wt%Si were equilibrated with pure SiO<sub>2</sub> crucibles under a helium atmosphere at 1550 °C. After one hour at temperature, the melts were quenched in hydrogen jets at rates of 7 - 10°/sec.

Series Ib; Iron melts containing 0.0 to 0.40 Wt%Si were equilibrated with SiO<sub>2</sub> crucibles at 1550 °C as in the previous series but were quenched by means of a cold copper plug at rates which varied from 30 to 300 °/sec across the ingot.

Series II; Iron melts containing 0.0 to 0.40 Wt%Si were equilibrated with SiO<sub>2</sub> crucibles at 1650 °C and quenched at various rates as described on page 65

During the runs in each of the series the temperature of the melt was recorded every five minutes by means of an optical pyrometer. Temperature fluctuations were seldom more than 5 °C and were readily detected by the total radiation pyrometer. The deviations were corrected by a slight adjustment of the power input to the coils.

In series Ia quench rates were calculated from the total radiation pyrometer data as recorded on the Honeywell strip chart. From the slope of the time - temperature line one could determine the quench rate at the ingot center to within ± 5 °/sec. The quench rates at the ingot edges of course

were much higher due to the proximity of the hydrogen jets.

In Series Ib, in which copper plugs were used, the quench rates were much higher. Recoalescence in each case could not be detected. The time - temperature profiles were much steeper and thus it was more difficult to accurately determine the quench rate. Rates were determined to within  $\pm 10^{\circ}$ /sec. Again, it was difficult to ascertain an average quench rate due to a gradation of rates across the ingot, the rate at a given point being a function of its distance from the copper plug. It may suffice to say that the rates in Series Ib were approximately 10 times higher than those in Series Ia.

An estimation of the time for liquid - solid transformation was made for each of the series. In the slow quench series this could be determined from the length of the solidification halt in the cooling curves. An average time of  $25 \pm 5$  seconds was observed. Another method was also used. Flemings<sup>32</sup> presents a plot of secondary dendrite arm spacing versus local solidification time for various alloys. The plot was adjusted by a geometric factor, as determined by Poirier,<sup>33</sup> to read in terms of primary dendrite spacing. The primary dendrite spacings in ingots from the slow quench series varied from 25 microns near the ingot edge to 100 microns at the ingot center which, from Fleming's plot, indicated local solidification times of 4 to 50 seconds. In the fast quench series primary

dendrite spacings varied from 10 microns near the copper plug to 60 microns near the ingot edge. These spacings corresponded to solidification times of 0.2 seconds and 20 seconds.

### A. OPTICAL OBSERVATIONS OF POLISHED SECTIONS

The results of observations of polished sections from ingots prepared in Series I are summarized in Table 11. Shown in the table are the chemical analyses of the ingot, the method of surface preparation and some general observations such as the types, sizes and distribution of particles present as observed in ordinary and polarized light.

The column marked  $f_s$ , indicates the fraction of metal solidified before the appearance of primary grain boundary particles. This value was obtained in the following manner. Consider the inclusions in a microsection of an ingot surface appearing as is shown in Figure 25.

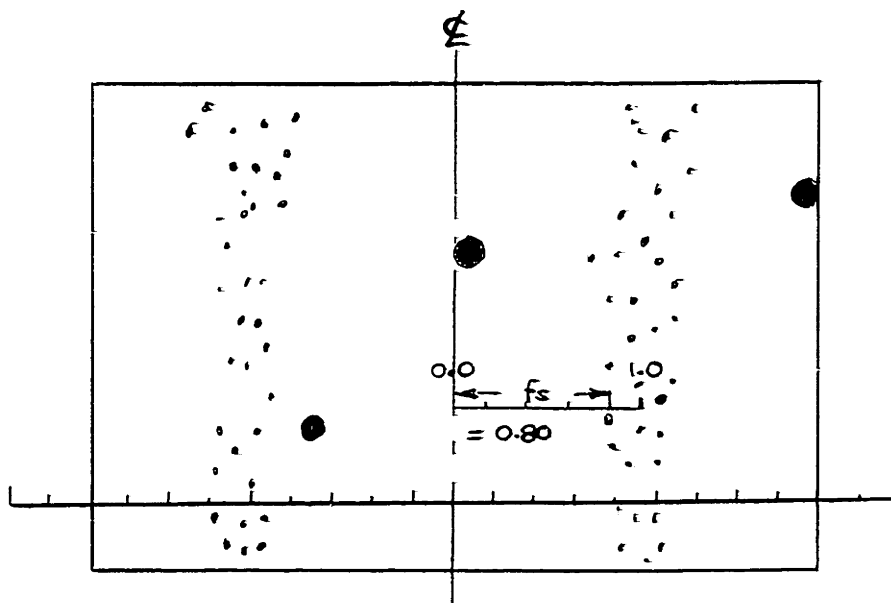


Figure 25: Evaluation of  $f_s$



The procedure was to place a Vernier scale across the microscope viewing screen and to record the positions of the center line and the boundary lines of the dendrite. Then a value representing the distance from the center line to the start of boundary particle population was recorded. This distance was calculated as a fraction of the center line to dendrite boundary distance and tabulated as  $f_s$ . Numerous measurements of this sort were made on a single ingot cross section from which an average  $f_s$  was calculated and recorded in Table 11.

#### 1. Series Ia - 1550°C - Slow Quench

The inclusions observed in polished ingot sections from this series were of two distinct types; large spherical inclusions located at random across the ingot, and smaller and more numerous inclusions situated at the dendrite boundaries. Also, the optical properties of these inclusions changed markedly with total silicon content of the ingot. A distinct change in the properties of the inclusions was observed at approximately 0.010 Wt% silicon.

Ingots having less than 0.010 Wt% total silicon: All inclusions in ingots in this concentration range were spherical in shape, light grey in color and opaque in polarized light. Their properties were characteristically those of FeO. Only a few random particles were observed. The vast majority of the inclusions were located at the dendrite boundaries as shown in Figure 26.



Figure 26: 500X Mechanical Polish. FeO Type Inclusions in Ingot 99. 0.006 Wt% Si.

Ingots having greater than 0.010 Wt% total silicon; All particles, both random and grain boundary, in ingots having greater than 0.010 Wt% total silicon appeared glassy in nature. In reflected white light the random larger inclusions were, for the most part, spherical and seemingly transparent. In polarized light the particles were bright and yellowish in color exhibiting the crossed Nicols effect typical of silica glasses . A typical particle is shown in Figure 27.

Occasionally these random inclusions were rosette-like in shape which when observed in polarized light appeared bright and diffuse and often green to reddish in color. Rosettes of this nature have been observed by numerous investigators, none of whom have successfully explained their

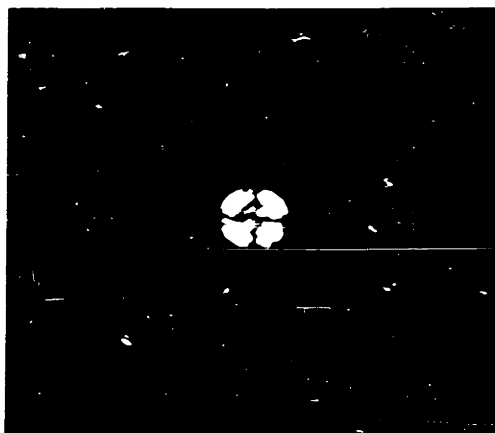


Figure 27: 1000X Electropolished. Silica Type Particle in an Iron Matrix.

occurrence. Fisher and Wahlster<sup>15</sup>, for example, suggested that silica spheres grew from a coalescence of many smaller silica particles and that a rosette represented an intermediate step in this growth process. They presented a series of microphotographs of inclusions portraying the development of the silica sphere. The group symmetry of the inclusions observed in polished sections indicated that they may in fact be the arms of a rosette, and not independent particles. To demonstrate this a metal surface containing rosettes was carefully polished and photographs of a particular rosette were taken at various stages of the polishing process. The sequence is shown in Figure 28.



Figure 28: 1000X Sections through a Rosette-type Inclusion.

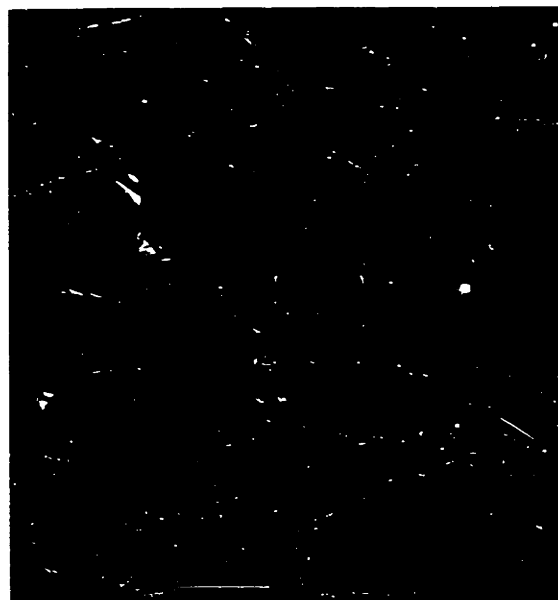
Although this series of photos taken from a single particle does not refute the argument by Fischer and Wahlster, it does indicate that an explanation for the mechanism of growth of silica particles based solely on observations of this nature could indeed be in error.

Turpin reasoned that rosettes were in fact saturated silicates, the core of the particle being a mixed silicate and the arms equilibrium silica that had been squeezed into that position during the solidification of iron. Still others<sup>34</sup> explain their appearance to be the result of surface instability caused by rapid cooling. Unfortunately, from the results of this study, it was impossible to support or deny any of the suggested explanations. The occurrence of these particles was completely unpredictable, their presence being detected in ingots quenched at various rates and containing from 0.010 to 0.20 Wt% silicon.

The majority of the inclusions observed in ingots from Series Ia were situated at the dendrite boundaries. The boundary inclusions, like the random precipitates, were glassy in character appearing bright in polarized light and red, green or colorless. Typical cross sections are shown in Figure 29.



Ordinary Light



Polarized Light

Figure 29: 200X Electropolished. Cell Boundary Precipitates in Ingots with Greater than 0.010 Wt%Si - Ingot 52

Of interest was the rod-like nature of the precipitates as observed in electropolished surfaces. The silicate inclusions were apparently not attacked by the electrolyte and with continued polishing, rods of approximately  $1\mu$  width and lengths up to  $100\mu$  were exposed. Some examples are shown in Figure 30.



Figure 30: 500X Electropolished. Rod-Like Grain Boundary Inclusions - Ingot 53; 0.012 Wt% Si.

The rods shown in Figure 30 were projected upwards from the metal surface. This was evidenced by lowering the specimen slowly towards the objective piece of the microscope and observing that the rod ends came into focus before the metal surface.

Inclusions of this nature were observed to a limited extent by Hilty and Crafts<sup>9</sup> and were described as an iron-silica eutectic, formed in the last of the liquid to solidify. According to Chadwick<sup>35</sup> rod-type eutectics of of this sort will form when the impurity in the liquid has appreciably different distribution coefficients for the two solid phases that are forming. In this case, silicon and oxygen have a much greater solubility in the silicate phase than in solid iron. During solidification the silicate phase grows into the liquid ahead of the advancing iron interface causing the eutectic lamellae to break up into very small cells. The development of this type of structure is shown schematically by Chalmers<sup>36</sup>. See Figure 31.

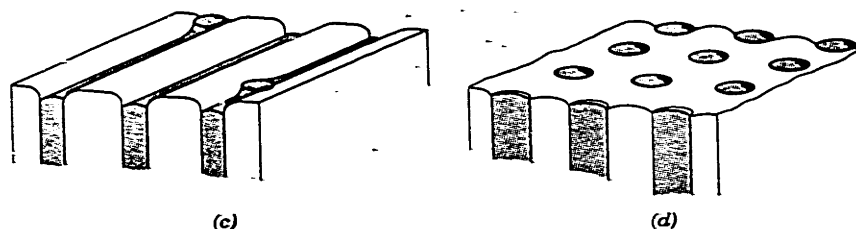


Figure 31: Origin of Rod-Type Eutectic



## 2. Series Ib - 1550°C - Fast Quench

To determine the effect of the faster quench on particle distribution, type and size, and to reduce growth processes to a minimum, a "rapid quench" series was performed. The type of oxide precipitate observed in polished sections (whether glassy or opaque) as a function of the silicon content of the ingot was similar to that observed in Series Ia. The number of random glassy spheres in ingots with silicon contents greater than 0.010 Wt% was unchanged and their average diameters were only slightly reduced. The primary iron dendrites were much smaller and the inclusions at their dendrite boundaries were extremely fine and much more numerous than in the previous series. Figure 32 portrays a series of dendrite cross sections in a single ingot progressing from the area of very fast quench, adjacent to the copper plug, to the slower rates nearer the ingot edge.

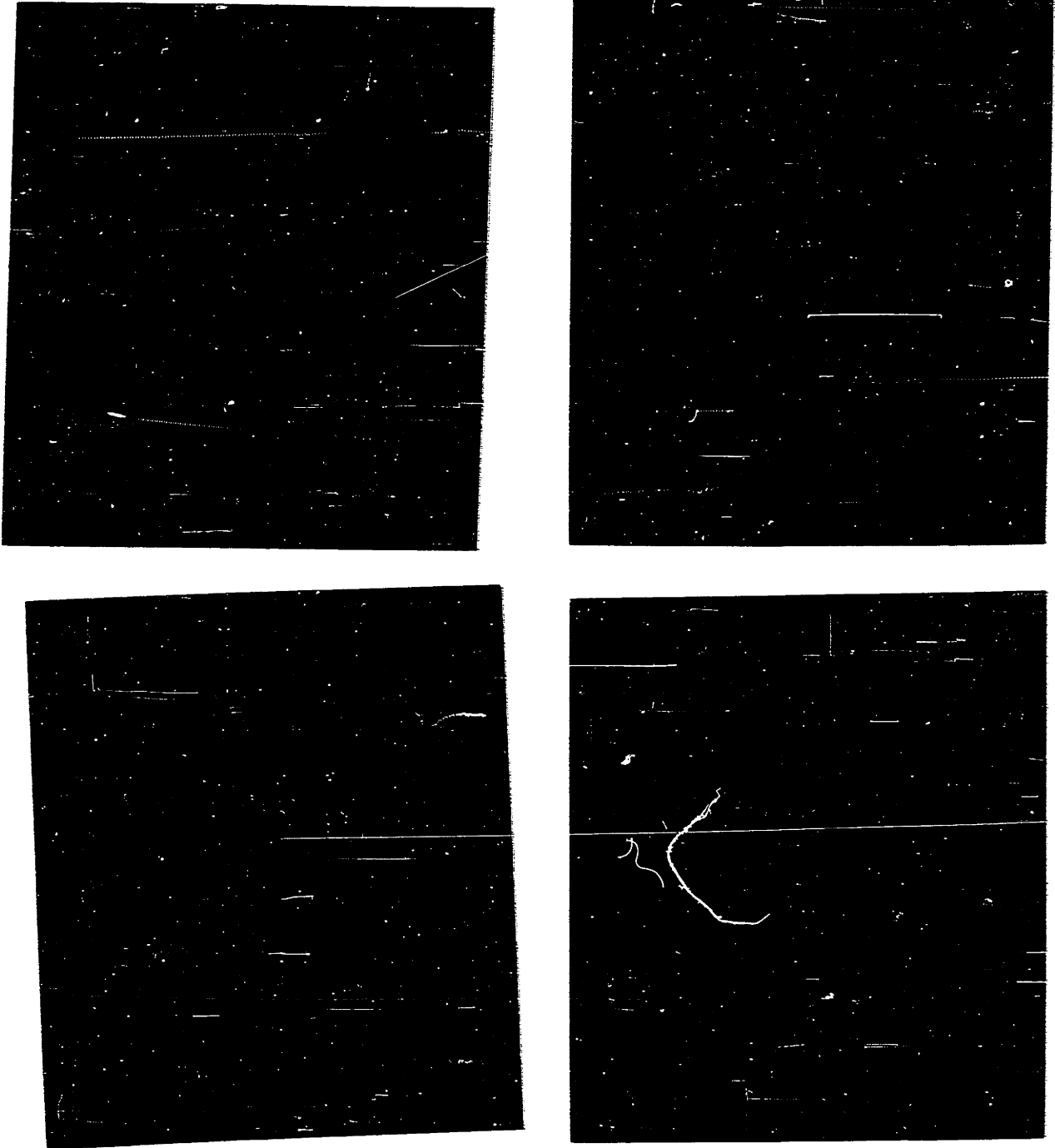
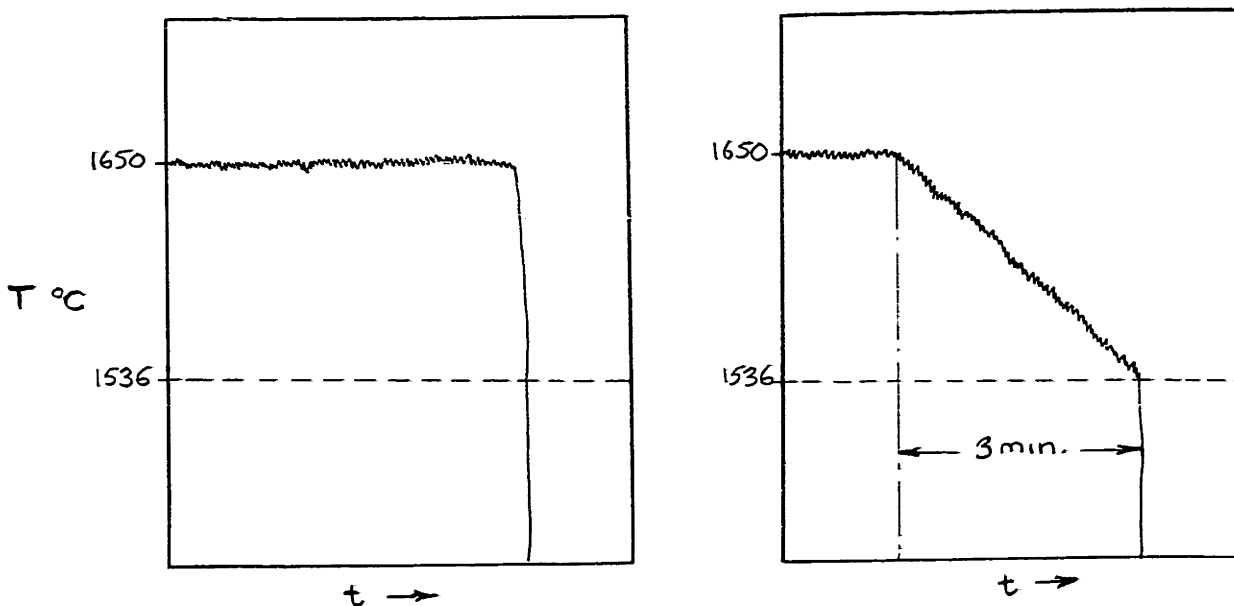


Figure 32: 1000X Mechanical Polish. Inclusion Type as a Function of Quench Rate - Ingot 107; 0.005 Wt% Si.

### 3. Series II - 1650°C - Fast and Slow Quench

As described in the previous sections on optical observations of inclusions in ingots quenched from 1550°C, there exist two types of inclusions; large spheres located at random in the iron matrix and more numerous and smaller particles situated at the dendrite boundaries. As noted from experiment the numbers of the former remain virtually unchanged with faster quench rates and their size was reduced only slightly. On the other hand, the size and numbers of the dendrite boundary precipitates were strongly a function of the quench rate indicating that the processes by which these two types of particles precipitated were dissimilar. Other investigators<sup>14,17</sup> have observed these particles and have reasoned that the random particles were formed during cooling of the iron liquid above the melting point of iron and the dendrite boundary particles were formed during solidification. To test this hypothesis a few runs were carried out at 1650°C and were quenched at differing rates as shown in Figure 33.

Ingot 126, which contained 0.20 Wt%Si, was equilibrated at 1650°C with a silica crucible and was quenched rapidly as in Series Ib from this temperature. Ingot 127, containing a similar initial silicon content, was equilibrated under the same conditions as ingot 126. However the quench sequence was different. Instead of plunging the copper plug



**Figure 33:** Time - Temperature Profiles Showing the Quench Sequences for Runs 126 and 127.

into the melt at 1650 °C, the power to the induction coils was gradually turned down allowing the melt to cool slowly over a period of three minutes to 1538 °C. At 1538 °C, or just above the melting point of iron, the power was turned off and immediately the copper plug was inserted into the melt.

Microscopic observations of ingots from this series are shown in Table 13. Figures 35 and 36 are photographs by polarized light of the ingot surfaces from runs 126 and 127. Shown for comparison (Figure 34) is a cross section of ingot 125 from Series Ib which contained a similar silicon content and was rapidly quenched from 1550 °C.

The sizes and distributions of the particles in the cross section of ingot 125 were typical of those observed in

Series Ib. Ingot 126, however, contained larger and more numerous random spheres. This increase in inclusion content is attributable to the increased solubility of silicon and oxygen at the higher temperature and was detected by an inclusion count performed with a quantitative television microscope . The inclusion counts are shown in Table F-1. None of the random particles were present in the cross section of ingot 127 and only dendrite boundary precipitates could be observed.

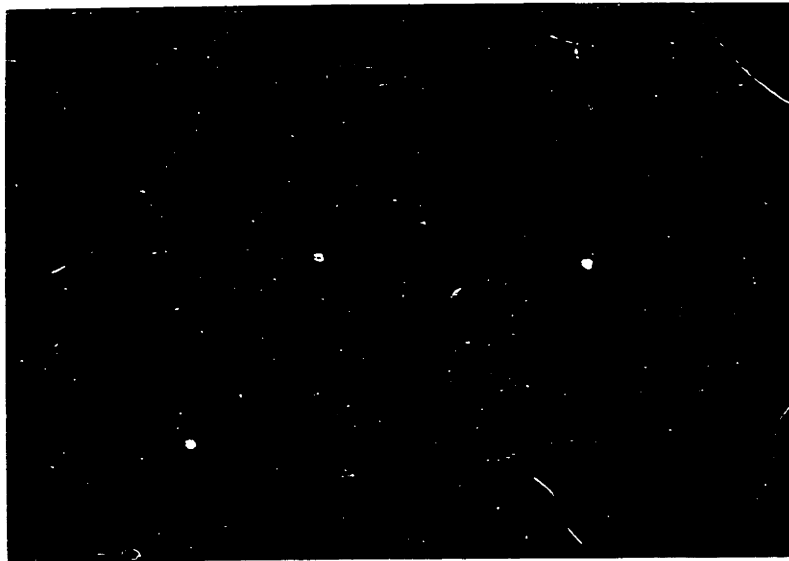


Figure 34: 175X Electropolished. Fast Quench from 1550°C -  
Ingot 125; 0.160 Wt% Si.

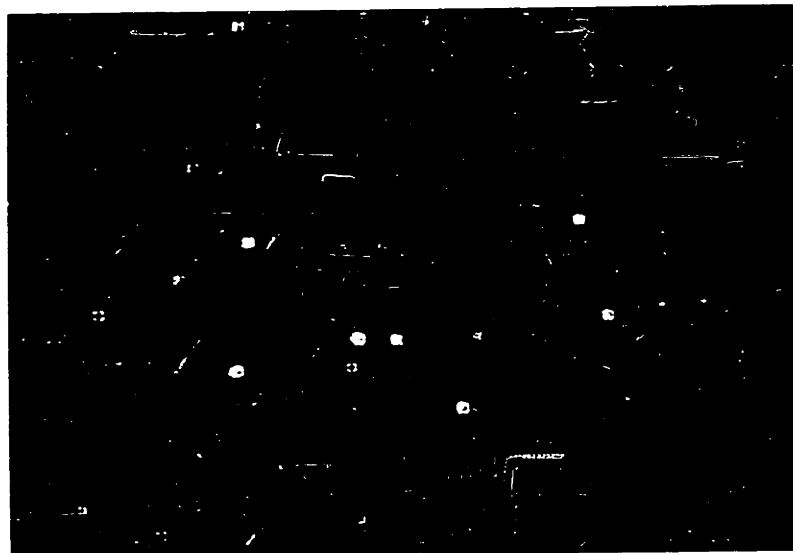


Figure 35: 175X Electropolished. Fast Quench from 1650°C -  
Ingot 126; 0.087 Wt% Si.

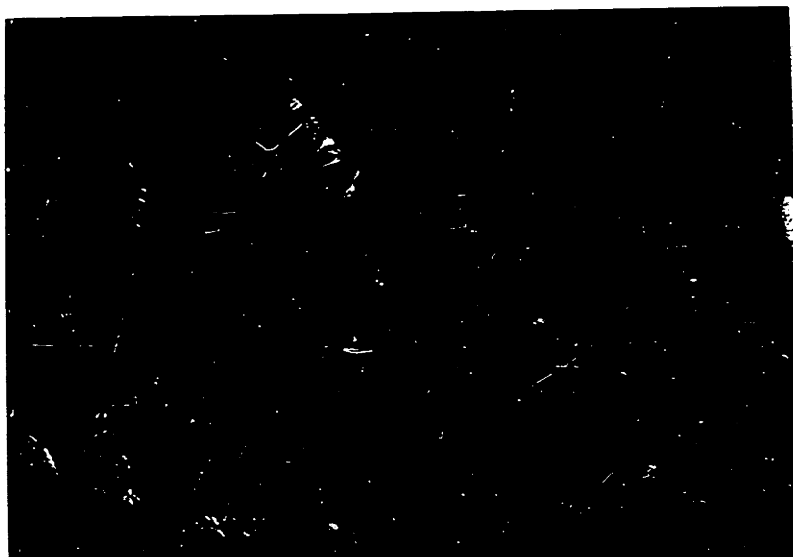


Figure 36: 175X Electropolished. Slow Cool from 1650°C to  
1538°C, Fast Quench from 1538°C - Ingot 127;  
0.21 Wt% Si.

The random particles from ingot 127 had floated to the surface of the liquid during slow cooling and were located at the upper corners of the ingot cross section as shown in Figure 37.



Figure 37: 500X Mechanical Polish. Silica Inclusions at Top of Ingot 127; 0.21 Wt% Si.

It is concluded from these experiments that the larger spherical precipitates situated at random in a rapidly quenched ingot are formed during cooling of the melt above the melting point of iron. If the cooling period is sufficiently long these particles will float to the ingot surface. All deoxidation products formed during the solidification of iron appear at the boundaries of the primary grains.

The summaries of the optical observations for the series Ia, Ib and II are shown in Tables 11, 12 and 13.

#### 4. Series II (Continued) - High Oxygen Ingots

Several melts in Series II were equilibrated with a silica saturated slag. This was achieved by admitting oxygen into the reaction chamber a few minutes after melt-down. After two minutes the oxygen port was closed and the melt equilibrated at 1650°C for forty-five minutes. The melt was then quenched rapidly with the copper plug.

The vast majority of the inclusions in ingots from this series were an Fe-FeO eutectic that appeared at the dendrite boundaries. The random particles, however, were much larger than those observed in the 1550°C series and consisted of more than one phase. See Figure 38.

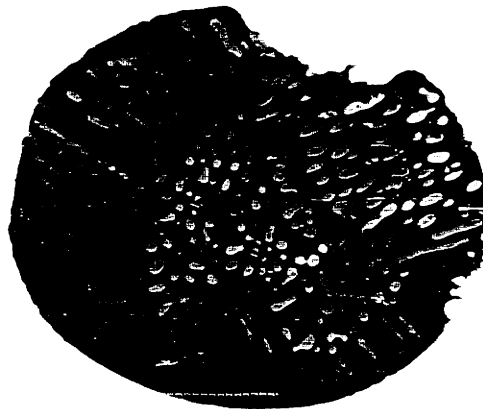


Figure 38: Complex Random Inclusion Appearing in High Oxygen Ingots Quenched from 1650°C. Ingot 119; 0.025Wt% Si.



Inclusions of this nature were observed by Herty<sup>7</sup>. He identified the light gray particles as FeO, and the surrounding dark gray matrix as an FeO-Fayalite eutectic. With the aid of Figure 39, one can explain the occurrence of particles of this nature.

Consider an iron melt at 1650°C of composition "X" in Figure 39. This point corresponds to silica saturation as calculated in Appendix A and is at 0.007 Wt% O and 0.10 Wt% Si. If this liquid is now cooled, liquid of composition "L" precipitates (silica saturated slag). As the liquid iron is cooled further the solubilities of oxygen and silicon in the liquid continue to decrease, however, due to the stoichiometry of the system (the decrease in the Wt% silicon is much less than the decrease in the Wt% oxygen) the compositions of the liquid slag "L" moves towards a higher O/Si ratio as shown in Figure 40. Simultaneously the composition of the liquid iron moves towards point "Y" in Figure 39. At point "Y", iron begins to solidify trapping the liquid slag in the iron dendrites. The balance of the oxygen precipitates as an Fe-FeO eutectic in the last of the liquid iron to solidify.

The process of solidification of the liquid slag may be followed using Figure 40. As the liquid slag is cooled to a temperature somewhat below 1372°C, it encounters the FeO liquidus surface at which point FeO particles begin to solidify. As FeO precipitates and grows, the composition of the remaining liquid moves from Point "m" to "n". At Point "n", the surrounding liquid precipitates as an FeO-Fayalite eutectic.

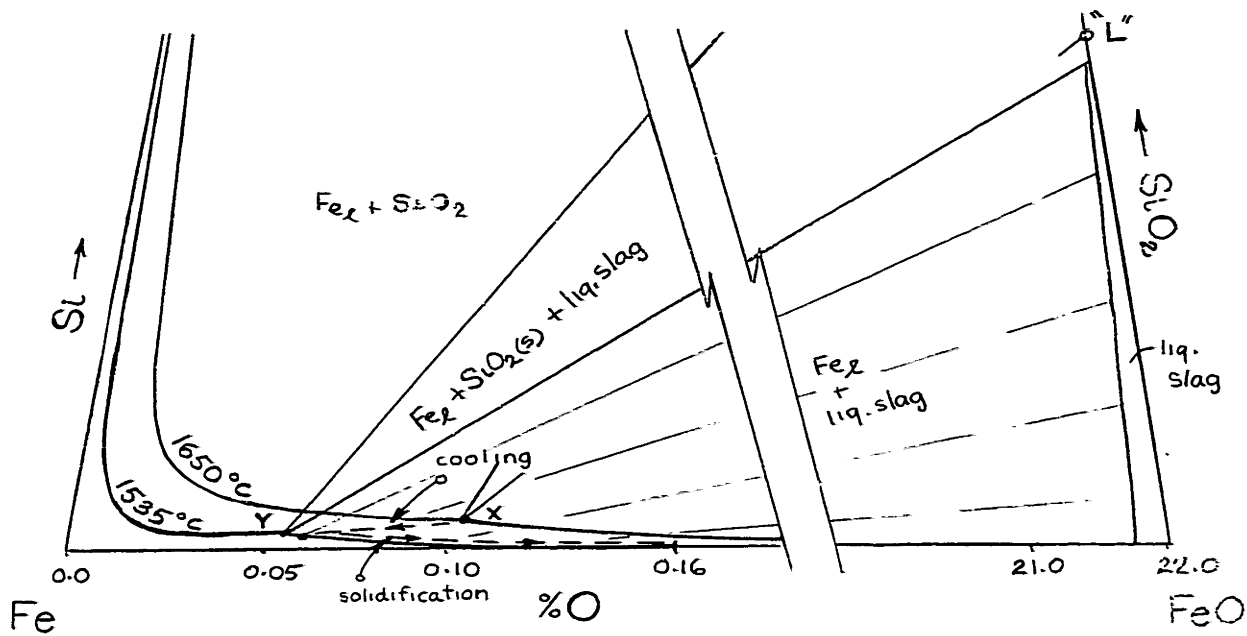


**Figure 39:** Cooling and Solidification of Melts Originally at Silica Saturation - 1650 C.

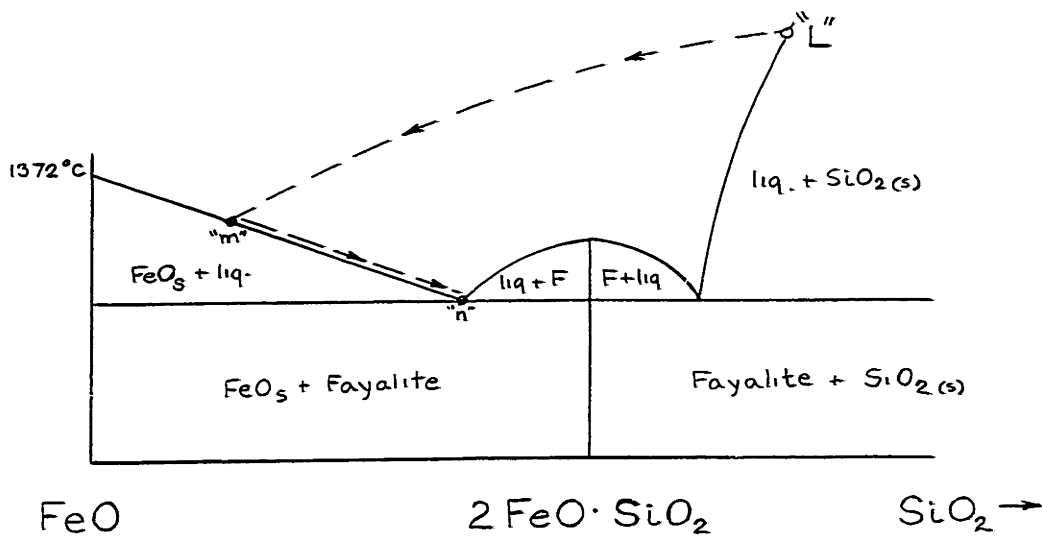


**Figure 40:** Cooling and Solidification of Liquid Slag "L"

TABLE 11: SUMMARY OF OPTICAL OBSERVATIONS ON QUENCHED SPECIMENS FOR SERIES Ia - 1550°C - SLOW QUENCH (H<sub>2</sub> JETS)

No.	Wt%Si	Surface Prep	Optical Properties		Random Precipitates		Grain Boundary Particles	
			Ordinary Light	Polarized Light	Avg $\phi(\mu)$	Comments	Avg $\phi(\mu)$	Comments
99	0.006	M.P.	light gray	opaque	15	spherical particles	0.9	small spheres
98	0.011	M.P.	"	"	11	"	0.8	"
53	0.012	E.P.	clear, glassy	bright	12	spherical, very few	1.0	rod-like eutectic
54	0.016	E.P.	"	"	13	spherical	1.0	"
61	0.016	E.P.	"	some colored	12	a few rosettes	1.0	"
62	0.018	E.P.	"	"	10	spherical	1.1	"
56	0.023	E.P.	"	"	10	fewer particles	1.0	"
52	0.032	E.P.	"	"	11	many rosettes	1.1	"
55	0.075	E.P.	"	bright, clear	12	spherical	1.2	eutectic, but sparse
49	0.092	E.P.	"	"	9	"	>0.95	rod-like eutectic
46	0.098	E.P.	"	"	9	very few	1.0	small amt. of eutectic
57	0.126	E.P.	"	"	7	medium number	1.1	"
48	0.160	E.P.	"	"	8	"	1.0	"
125	0.160	E.P.	"	"	10	spherical	1.0	rod-like eutectic
60	0.176	E.P.	"	"	5	very few	1.0	small amt. of eutectic
63	0.211	E.P.	"	"	10	"	1.0	"
50	0.250	E.P.	"	"	5	"	0.9	very little eutectic
58	0.342	E.P.	"	"	4	"	0.9	"
51	0.376	E.P.	"	"	5	"	1.0	"
59	0.564	E.P.	"	"	7	"	0.9	"
64	0.702	E.P.	"	"	6	"	0.9	"

Surface Preparation

M.P. - Mechanical Polish

E.P. - Electropolished

TABLE 12: SUMMARY OF OPTICAL OBSERVATIONS ON QUENCHED SPECIMENS FOR SERIES Ib - 1550°C - FAST QUENCH (COPPER PLUG)

No.	Wt%Si	Sur-face Prep	Optical Properties		Random Precipitates		Grain Boundary Particles		Comments
			Ordinary Light	Polarized Light	Avg $\phi$ ( $\mu$ )	Comments	Avg $\phi$ ( $\mu$ )	f s	
103	0.002	M.P.	light gray	opaque	10	spherical	0.5	0.78	particles smaller near plug, spherical
114	0.002	M.P.	"	"	9	spherical, very few	0.6	0.81	"
104	0.004	M.P.	"	"	10	spherical	0.5	0.85	"
107	0.005	M.P.	"	"	8	"	0.5	0.83	"
113	0.007	M.P.	"	"	10	"	0.6	0.86	"
108	0.008	M.P.	"	"	11	"	0.7	0.80	"
109	0.016	E.P.	clear, glassy	bright, colored	10	some rosettes	0.5	0.91	short rods visible
101	0.017	E.P.	"	"	9	many rosettes	0.4	0.95	rod-like eutectic
105	0.040	E.P.	"	bright	10	spherical	0.5	0.95	"

Surface Preparation

M.P. - Mechanical Polish

E.P. - Electropolished

TABLE 13: SUMMARY OF OPTICAL OBSERVATIONS ON QUENCHED SPECIMENS FOR SERIES II - 1650 °C

No.	Wt%Si	Qu. Seq*	Optical Properties		Random Precipitates		Grain Boundary Particles		Comments
			Ordinary Light	Polarized Light	Avg $\phi(\mu)$	Comments	Avg $\phi(\mu)$	f s	
121	0.006	s-f	light gray	opaque	20	segregated towards top - two phases	0.5	0.75	small, spherical
122	0.006	s-f	"	"	19	"	0.5	0.70	"
120	0.011	s	"	"	20	two phases	0.9	0.75	"
116	0.016	s	"	"	13	"	1.0	0.80	"
119	0.025	s	"	"	18	"	1.0	0.79	"
118	0.052	s	"	"	20	"	0.8	0.83	"
115	0.068	f	clear	bright	8	spheres	0.5	>0.95	rod-like eutectic
123	0.086	f	"	"	11	many rosettes	0.6	"	"
126	0.087	f	"	"	10	many spheres and rosettes	0.5	"	"
124	0.090	s	"	"	8	many spheres	0.8	"	"
127	0.210	s-f	"	"	9	all at ingot surface	0.5	"	"

\*s, - slow quench H<sub>2</sub> (jets)

f, - fast quench Cu (plug)

s-f, - slow cool, fast quench

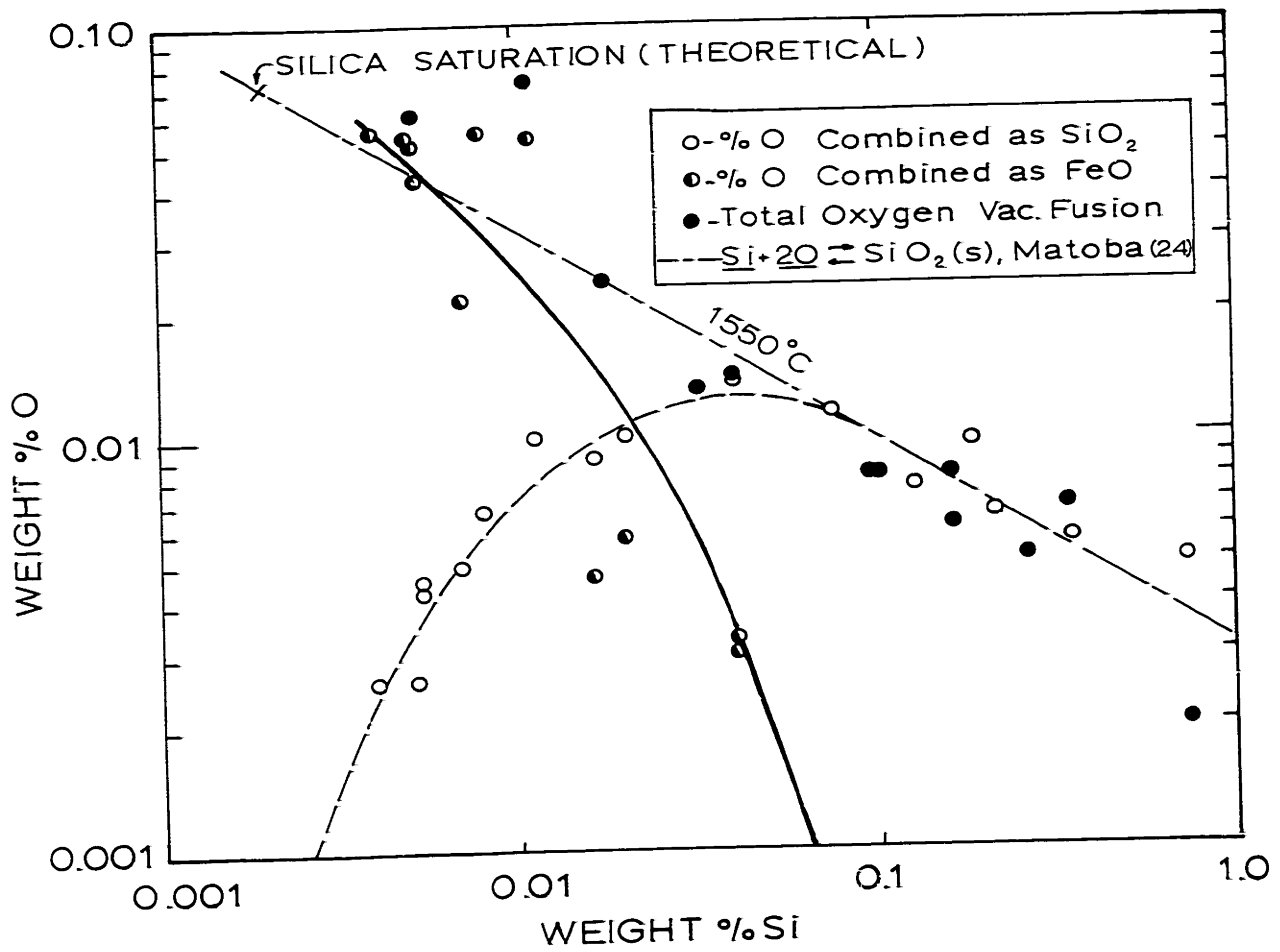
## B. IDENTIFICATION OF INCLUSIONS

To provide assistance in the evaluation and interpretation of the processes by which inclusions are formed during cooling and solidification of liquid iron, a program of analysis was undertaken to determine the chemical compositions and structures of inclusions in the iron ingots. Inclusions from ingots containing 0.008 to 0.71 Wt% total silicon from both the slow and the fast quench series were extracted and analyzed. Electron probe analyses of the inclusions in situ were performed as a qualitative check of the validity of the extraction analyses. The details of the extraction procedure are presented in Appendix C.

### 1. Extraction and Chemical Analysis of Inclusions

As described in Appendix C, inclusions were extracted and analyzed to determine their iron and silicon contents. The total oxygen content of the ingot was then calculated assuming all oxygen to be present as FeO and/or SiO<sub>2</sub>. These values were checked by determining the total oxygen content of the ingot from vacuum fusion analysis.

The results of the chemical analysis of extracted inclusions from melts quenched from 1550°C are shown in Figure 41. The full circles are those points determined from total silicon analysis and total oxygen analysis. The straight line is the silica equilibrium line for 1550°C as determined by Matoba<sup>24</sup>. The half-filled circles show the percentage oxygen combined as FeO and the clear circles the percentage oxygen combined as SiO<sub>2</sub>.



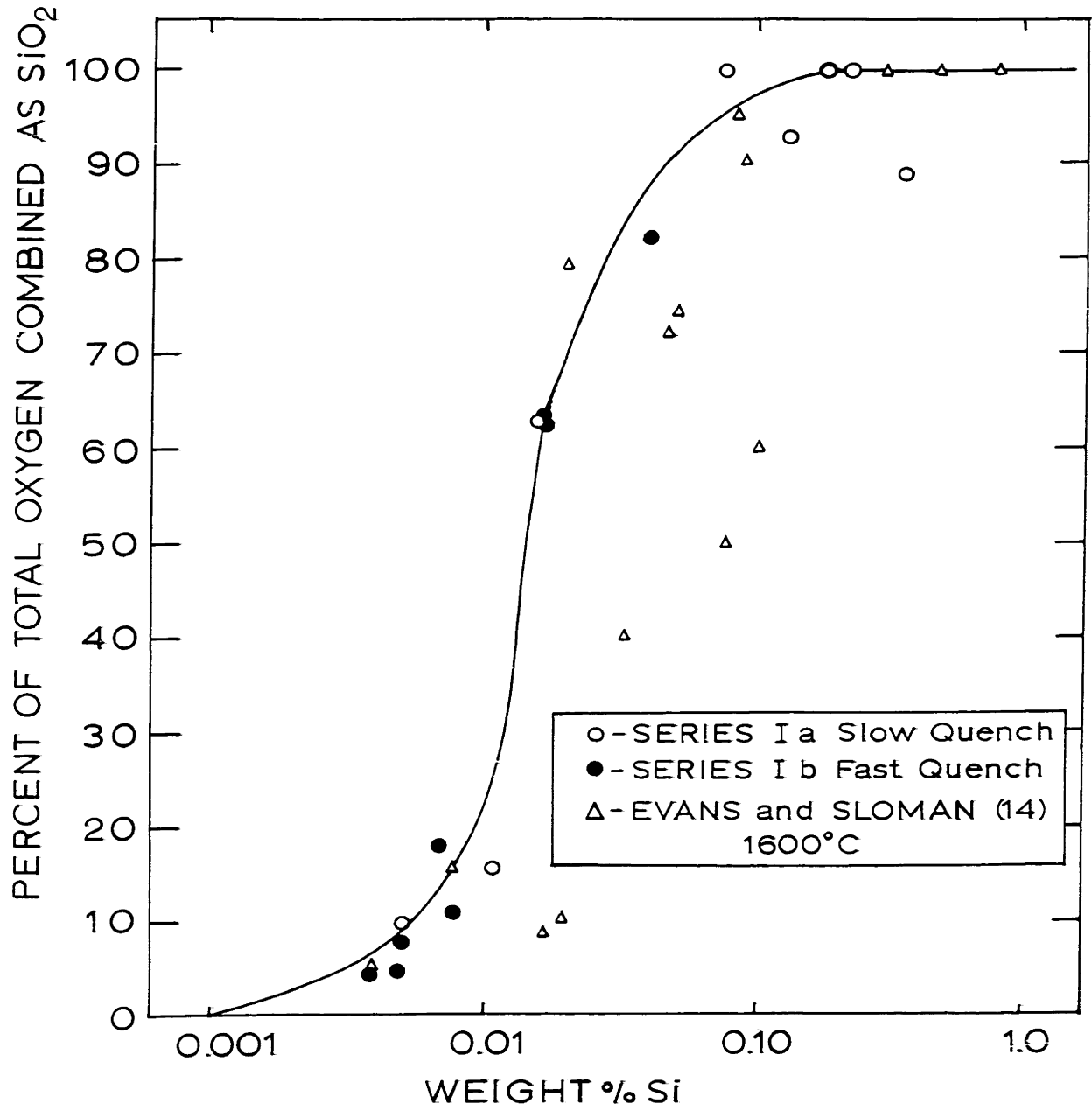
Results of Chemical Analysis of Extracted Inclusions

FIGURE 41

An upper limit to the equilibrium oxygen potential in iron was observed and was situated in the range 0.060 to 0.070 Wt% total oxygen. This limit corresponds to an invariant iron composition defined by silica saturation, which in the course of the experiments, was evidenced by severe crucible attack. The theoretical point of silica saturation, as calculated in Appendix A is shown for comparison and is at 0.0015 Wt% Si and 0.063 Wt% O. Some scatter in experimental results in this range is evident and is due largely to difficulties encountered in analyzing low silicon contents. At best, silicon concentrations in iron can be determined colorimetrically to within  $\pm 0.002\%$ . However, the largest error in analysis is probably due to the inability to prepare an iron sample which does not have adhering or entrained crucible fragments.

The results of the extraction study, as shown in Figure 41, indicate that, for ingots containing below 0.01 Wt% total silicon, virtually all of the oxygen is present as FeO inclusions. Above this value there is a sharp increase in the SiO<sub>2</sub> content of the particles and for ingots containing greater than 0.09 Wt% silicon all of the oxygen is combined as SiO<sub>2</sub>. This change in particle composition is shown in Figure 42 where, the percent of the total oxygen as SiO<sub>2</sub> is shown as a function of the total silicon content of the iron. Analyses from both the fast and the slow quench runs are shown and would indicate that the compositions of the inclusions are not





Percentage of Total Oxygen Combined as  $\text{SiO}_2$  vs Si

FIGURE 42

strongly influenced by the rate of solidification of the sample.

## 2. X-Ray Diffraction of Extracted Inclusions

Debye - Scherrer X-ray patterns from oxide inclusions extracted from three ingots are shown in Figure 43. Strong lines were obtained from the residue of ingot 103 containing 0.002 Wt% Si and were identified as FeO. The lines from ingot 109 containing 0.017 Wt% Si were very faint showing some FeO lines and a few low index lines possibly corresponding to a form of cristobalite. No lines could be detected in the high silicon ingot indicating that the SiO<sub>2</sub> particles were glassy.

## 3. Electron Diffraction.

Similar results were obtained when the residues from the three ingots were examined by electron diffraction. The black residue from ingot 103 exhibited a Transmission Laue pattern characteristic of a cubic material as shown in Figure 44. Due to distortion effects the pattern was rather difficult to index but by comparison with a standard gold pattern it was identified as FeO. The pattern disappeared after a few seconds of electron bombardment, probably because of decomposition of metastable FeO in the high energy electron beam. No diffraction pattern was observable for residues from ingots 109 and 106.



No. 103 .002 Wt% Si

Cr Rad. 35 K.V.  
15 m.a.  
1½ hrs

Identification: FeO



No. 109 .017 Wt% Si

Cu Rad. 35 K.V.  
15 m.a.  
1 hr

Identification: Some Cristobalite?  
Glass



No. 106 .28 Wt% Si

Cu Rad. 35 K.V.  
15 m.a.  
1 hr

Identification: Glass

Figure 43: X-Ray Diffraction Patterns of Extracted Inclusions  
from Ingots 103, 109 and 106

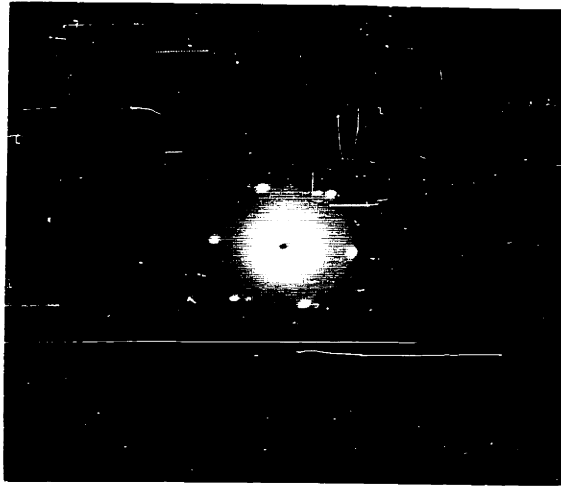


Figure 44: Electron Diffraction Pattern of FeO Inclusions from Ingot 103; 0.002 Wt% Si.

#### 4. Electron Probe Analysis

To check qualitatively whether this change in  $\text{SiO}_2$  content of inclusions in the range 0.01 to 0.10 Wt% Si could be observed in minute dendrite boundary particles, electron probe traces were taken across several dendrites adjacent to the copper plug (in the region of fastest quench) in ingots 108 and 105. The radiation recorded was Silicon  $K_\alpha$ . The traces are shown in Figures 45 and 46.

The trace across particles in ingot 108, .008 Wt% Si, shows no significant fluctuation in Si  $K_\alpha$  radiation. However, very definite peaks were encountered in traversing particles in ingot 105, 0.04 Wt% Si, indicating that the compositions changes determined by the extraction technique occur in even the smallest particles. Quantitative estimates of the amount of silicon in the particles could not be made by this method as the area of the probe beam was greater than that of the particle.

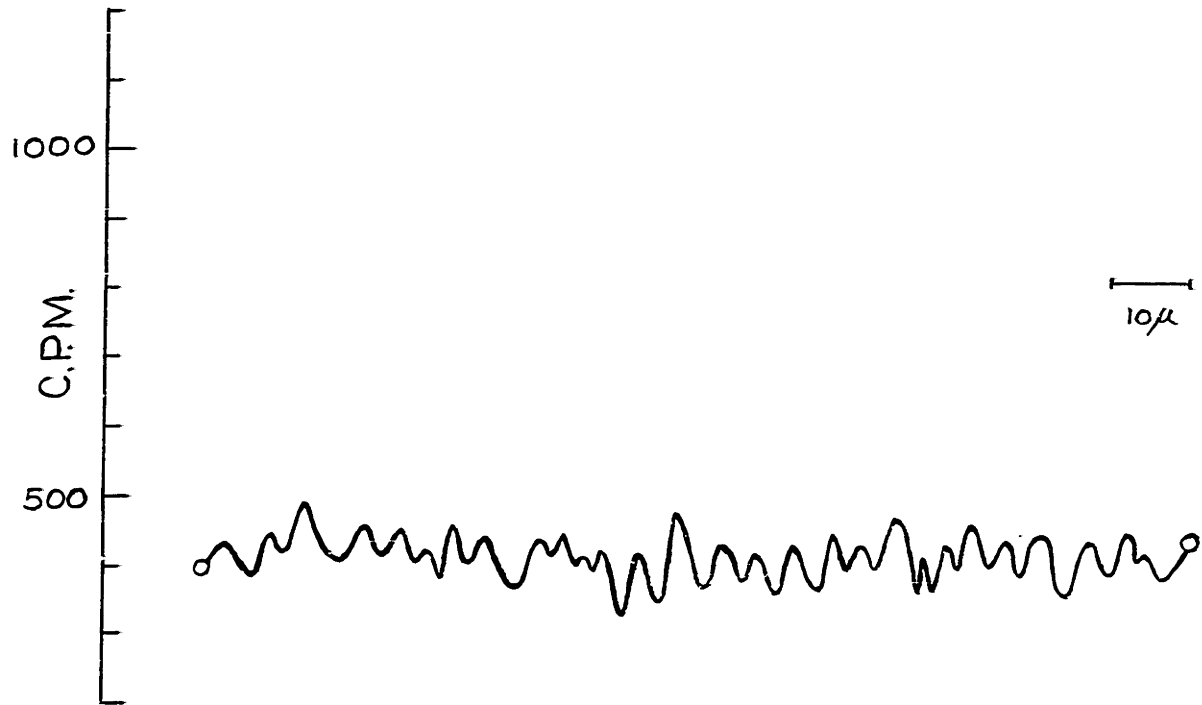


Figure 45: Electron Probe Trace for Si  $K_{\alpha}$  Radiation Across Inclusions in Ingot 108; 0.008 Wt% Si.

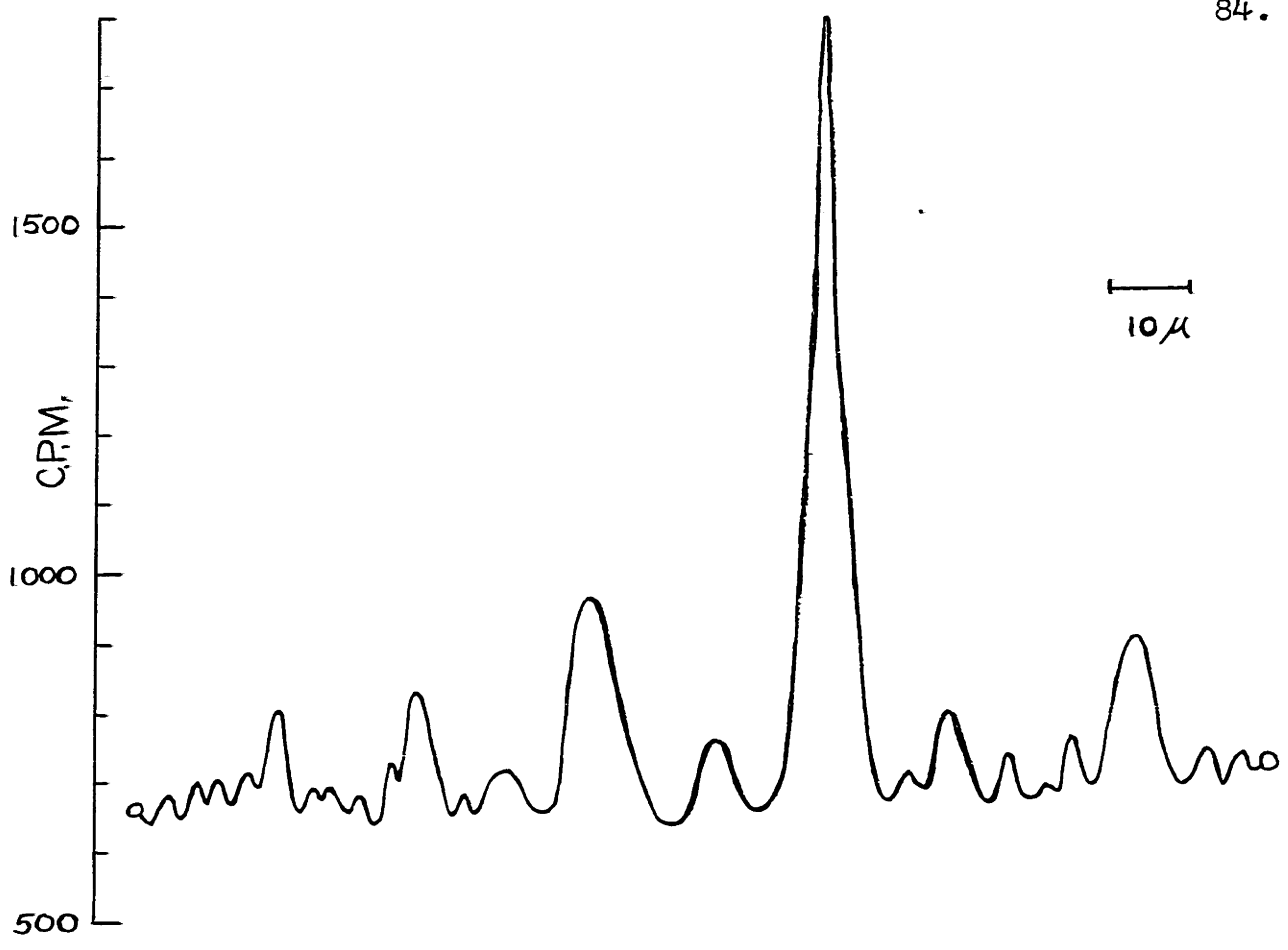


Figure 46: Electron Probe Trace for Si K<sub>α</sub> Radiation Across Inclusions in Ingot 105; 0.04 Wt% Si.

## VI. DISCUSSION

In section III several possible processes by which oxide phases precipitate during the solidification of iron were considered. Two models representing "Barrier Free" and "Barrier" solidification were constructed - Models I and II. The process of solidification of various liquids in the Fe-Si-O system was then considered, and for each model, the resulting distributions of the inclusions in the solid metal section and the inclusion compositions were determined. Summaries of these calculations are given on pages 34 and 42. To test these models, a series of solidification experiments was performed, the results of which are described in section V. An analysis and interpretation of the experimental results in terms of the solidification models follows.

### A. Location of Inclusions

Experimental results from this study show that inclusions formed during the solidification of iron precipitate in the very last portion of the liquid iron to solidify and appear, in the solid section, at the dendrite boundaries. The clearest evidence of this behaviour was observed in Series II, in which the distinction between inclusions formed during the cooling of liquid iron and those precipitated during solidification was made. The particles precipitated during cooling of the liquid were present as small spheres distributed at random in the solid section. Oxide inclusions formed during

solidification in ingots containing from 0.006 to 0.70 Wt % Si (series Ia) appeared at the dendrite boundaries corresponding to the last portions of the liquid iron to solidify - Table 11.

The locations of the inclusions observed in the solid sections correspond to those predicted from Model II. The model, based on classical nucleation, shows that, in the absence of nucleating substrates, supersaturation of the liquid in oxygen and silicon sufficient to cause homogeneous nucleation of the oxide phase is achieved only in the final stages of solidification. Oxide particles formed in this manner would appear at the dendrite peripheries. The excellent agreement between model and experiment can best be seen by comparing predicted inclusion distributions, Figures 16 -20, and those observed from experiment, Figures 26 and 29. By comparison, the inclusion distributions predicted from Model I -- Figures 10-14 -- are contrary to experimental evidence.

More specifically, Model II predicts, for ingots containing over 0.04 Wt% silicon, that supersaturations necessary for homogeneous nucleation of the oxide phase occur only when more than 96 percent of the iron has solidified - see Figure 21. In this range the agreement between Model II and experiment is immediately obvious - (Table 11). Evidence of supersaturation was somewhat more difficult to detect in ingots containing less than 0.010 Wt% silicon. If no barrier



to the nucleation of FeO exists, Model I predicts the appearance of an Fe-FeO eutectic when the iron is 60 percent solid. Conversely if no nucleating substrate is available then supersaturation must occur and from Model II it is predicted that FeO particles will not appear until 80 percent of the iron is solid. In this study the Fe-FeO eutectic appeared in the last 10 to 20 percent of the metal to solidify indicating the supersaturation did occur (see Table 12).

As mentioned earlier, experiments performed in series II indicated that certain of the inclusions observed in ingots quenched from high temperatures were formed during cooling of the melt and thus were present in the liquid at the onset of solidification. The rapid quench experiments performed in series Ib have shown that these particles are distributed at random in the solidified section. No segregation towards primary grain boundaries was observed (see Figure 35). This evidence lends further credence to the assumption that particles suspended in the liquid are not displaced by the advancing solid-liquid interface and supports the rejection of Model III.

The location of inclusions would also be affected by nucleation at the solid iron-liquid interface. In an analysis of the solidification process, Turkdogan<sup>16</sup> has assumed that the interface can indeed nucleate oxide inclusions at small supersaturations of silicon and oxygen. There is evidence to the contrary. Chalmers<sup>37</sup> noticed that, during the solidifi-

cation of water, air bubbles did not form as expected at the interface but in the liquid ahead of the interface. Turpin has considered this question with regard to nucleation of oxide inclusions during the solidification of iron. From an analysis of the interfacial tensions, using available surface tension data and estimates of crystal-solid substrate interfacial tensions given by Vonnegut and Turnbull<sup>40</sup>, he concludes that the work to create an oxide-solid interface is greater than that to produce an oxide-liquid interface. Thus, nucleation in the liquid will be preferred. Also, silica glass does not wet solid iron. This may also be said of liquid FeO. In all cases, FeO particles, even in areas of high concentration in solid iron sections, are observed to be perfectly spherical indicating that the contact angle between liquid FeO and solid iron is zero -(see Figure 26). Further, the locations of the inclusions in ingots from this study - Table 11 - indicate that nucleation did not occur at the solid-liquid interface. If the interface did in fact provide a substrate for nucleation, precipitation would occur throughout the solidification process and the oxide inclusions would appear at random across the iron dendrites.

It also may be argued that many oxide particles nucleate in the earlier stages of solidification and are located in the matrix of the dendrite but that they are submicroscopic in size. The excellent agreement between oxygen analyses

performed by vacuum fusion and those determined by the extraction procedure, (Table C-1), would indicate that this is not the case. The minimum pore diameter of the membrane filters used in the extraction was  $0.3\mu$ , a particle size within optical limits of the light microscope. Particles smaller than this would easily pass through the filter and the total oxygen as determined by the extraction process would be well below that analyzed by vacuum fusion.

#### B. Inclusion Compositions

The compositions of the oxide inclusions formed during solidification of iron as calculated from Model II using  $\sigma_{Fe_l - SiO_2} = 1300 \text{ ergs/cm}^2$  and  $\sigma_{Fe_l - FeO_l} = 250 \text{ ergs/cm}^2$  were consistent with those determined from experiment. Table 14 shows the percentage of the total oxygen combined as  $SiO_2$  for five liquids as calculated from the "Barrier Free" and "Barrier" models - Models I and II in section III. Also shown are the inclusion compositions determined from the extraction procedure. The values were obtained from Figure 42.

Initial Si in Liquid	% of Total O Combined as $SiO_2$	% of Total O Combined as $SiO_2$	% of Oxygen Total Combined as $SiO_2$
Wt %	Model I	Model II	Experimental
0.20	100	100	100
0.10	100	100	100
0.04	100	44	82
0.01	35	8	17
0.0015	0	0	0

Table 14: Compositions of Inclusions as Determined by Calculation and by Experiment

Of interest is the fact that Model II predicts that only in ingots containing greater than 0.10 Wt% total silicon will the inclusions be 100 percent silica, whereas Model I predicts this to occur at 0.04% total silicon. Experimental results from this study show that inclusion compositions approach pure silica only in ingots containing greater than 0.09 Wt% total silicon - see Figure 41. These observations are in agreement with those of Evans and Sloman<sup>14</sup> - Figure 42. Although one cannot accept or reject either model solely on this evidence of inclusion compositions, it is significant that the compositions determined experimentally can be anticipated from Model II using classical nucleation theory.

The preceding analysis of the experimental results show that inclusion compositions and their distributions in the solid section are best described by "Barrier" solidification - Model II. During the freezing of iron, considerable supersaturation of the interdendritic liquid takes place and nucleation of oxide inclusions does not occur until supersaturations necessary for homogeneous nucleation of the oxide phase are achieved. Sites for heterogeneous nucleation are rendered ineffective. An analogy between this behaviour and experiments on the supercooling of liquids may be made.

### C. Isolation of Nucleation Sites During Solidification

#### 1. The Supercooling of Liquids

Under certain conditions liquid metals may be supercooled to temperatures well below their melting point. It has been demonstrated that aggregates of small liquid droplets of tin<sup>38</sup>, mercury<sup>39</sup>, gallium<sup>40</sup>, bismuth and lead<sup>40</sup>, which are kept from intercommunicating by suitable films, do not solidify at an appreciable rate unless the supercooling is very much greater than that necessary to cause a large continuous mass of metal to solidify. For example, oxide-coated tin droplets<sup>38</sup> must be supercooled 100° to 110° C before their rate of solidification becomes rapid, although large continuous masses of liquid tin begin to solidify when supercooled 30° or less<sup>41</sup>.

The nuclei effective at small degrees of supercooling in the bulk metal are relatively few in number and are either internal or surface heterogeneities. If the metal is subdivided, those droplets that happen to contain such nuclei will solidify at a temperature not greatly below the true freezing point, but only a small fraction of the whole volume will be affected. The majority of the drops will undercool to a much lower temperature where nucleation occurs as a result of fluctuations.

Wang and Smith<sup>48</sup> propose that an appropriate subdivision to give effective freedom from random nuclei is produced during the solidification of many alloys that contain

a minor amount of a phase of lower melting point and that one might expect marked undercooling of the distributed phase. They observed, for example, that tin in an aluminum-tin alloy with 10 percent tin solidified over a temperature range as high as  $100^{\circ}\text{C}$ .

The above reasoning could help to explain the mechanisms by which oxide inclusions nucleate during cooling and solidification of liquid iron. Experimental evidence indicates that the precipitation of oxide phases during the cooling of liquid iron occurs readily requiring little or no supercooling. On the other hand, the results from this study show that during the solidification of iron large supersaturations of the interdendritic liquid are necessary to nucleate the oxide phase.

## 2. Cooling of Liquid Iron

Consider an iron melt at  $1600^{\circ}\text{C}$  in which silicon and oxygen are dissolved. If the liquid is now cooled there is a corresponding decrease in the solubility of the solutes. The liquid, during cooling, remains a large continuous medium and contains numerous nuclei that are distributed randomly throughout the liquid. These nuclei may be oxide particles precipitated at the higher temperature or minute crucible fragments. Thus, precipitation of the equilibrium oxide phase will be rapid and will take the form of either heterogeneous nucleation followed by a growth process or simple growth of the existing particles. Experiments performed by Turpin and Elliott<sup>17</sup>

indicate that, even under carefully controlled conditions, little if any undercooling of the oxide phase can be detected during cooling of iron melts.

Once nucleated, the oxide particles must grow extremely rapidly. Miyashita<sup>42</sup> estimates from a growth model based on collision theory that silica particles in an iron bath at 1600 C may grow from an initial particle diameter of  $10^{-6}$  cm to  $10^{-3}$  cm in as little as  $10^{-2}$  seconds\*. In this study silica particles of the order of 5-10 $\mu$  in diameter were observed in the area adjacent to the copper plug where quench rates of up to 300 °/second were achieved .

### 3. Solidification of Iron

The iron melt discussed in the previous section, now at 1536 °C and containing a suspension of oxide particles is allowed to solidify. During solidification long dendrites of solid iron grow into the melt rejecting silicon and oxygen into the interdendritic liquid. The diffusion path from an area of supersaturation next to a particular dendrite to a nucleus located somewhere in the dendrite network must now become longer and more complicated. Also, local convection in the interdendritic liquid is reduced by the presence of the dendrites thus diminishing the "sphere of influence" of a particular

---

\*Times of 0.75 seconds for iron containing 0.20 Wt% Si, and 15 seconds for iron containing 0.04 Wt% Si were calculated from a diffusion model proposed by Zener.<sup>43</sup>

nucleus. Lastly, during the freezing process, the random nuclei are continuously being engulfed by the growing dendrites rendering them ineffective. Hence, during solidification, the majority of the nuclei present in the liquid may become "isolated" from areas of interdendritic supersaturation. This reasoning would explain the large supersaturations observed experimentally.



## VII. SUMMARY AND CONCLUSIONS

The processes by which oxide inclusions form during the solidification of iron melts have been investigated. Various mechanisms were considered and two solidification models simulating the possible processes were constructed. Model I assumes easy nucleation of the oxide phase and melt-oxide equilibrium throughout the freezing process. Little or no supersaturation of the solutes in the liquid occurs. Model II assumes homogeneous nucleation of the oxide phases resulting in large supersaturations of the interdendritic liquid. Critical supersaturations for homogeneous nucleation were calculated from classical nucleation theory as adapted by Turpin and Elliott. For the case of iron containing oxygen and silicon, the interfacial tensions used were:  $\sigma_{\text{Fe}_\ell - \text{SiO}_2} = 1300 \text{ ergs/cm}^2$  and  $\sigma_{\text{Fe}_\ell - \text{FeO}_\ell} = 250 \text{ ergs/cm}^2$ . For each model inclusion compositions and their location in the solid section were determined.

Experiments were performed in which iron melts were equilibrated with silica crucibles then quenched. The ingots were sectioned and analyzed, and the distributions and nature of the inclusions in polished sections examined with the light microscope. Inclusions were extracted by a cold nitric acid technique and identified by gravimetric and colorimetric analysis, electron diffraction and X-Ray diffraction. Electron probe analysis of inclusions in situ was also performed. The

results were compared to those predicted from Models I and II.

The locations and compositions of the inclusions observed from experiment agree with those determined from Model II. In all cases, oxide inclusions which formed during the freezing of iron appeared in the form of a divorced eutectic at the primary grain boundaries corresponding to the last portion of the iron to solidify. Analysis of the inclusions showed that in ingots containing less than 0.010 Wt% silicon, the inclusions are pure iron oxide. In the range 0.01 to 0.09 Wt% silicon the inclusions are mixed silicates, and above 0.09 Wt% silicon all oxygen is combined as glassy silica.

The results indicate that during the solidification of iron containing silicon and oxygen, large supersaturations of the interdendritic liquid occur. The distributions and compositions of the inclusions are consistent with those calculated from classical nucleation theory indicating that nucleation of oxide inclusions during solidification of iron is homogeneous and takes place in the liquid iron ahead of the advancing solid iron-liquid interface.

## VIII. SUGGESTIONS FOR FURTHER WORK

### A. Solidification Studies in Other Systems

A solidification study, similar to this investigation, could be performed in the system Fe-Al-O. Sufficient equilibrium data is available<sup>44-46</sup> and Turpin<sup>17</sup> has analyzed the nucleation of oxides in this system in terms of classical theory. Thus, models representing "Barrier-Free" and "Barrier" solidification could be constructed.

Iron melts could be equilibrated with alumina crucibles then quenched. The distributions and compositions of the inclusions could be determined and compared to those predicted by the models. The crystalline phases in this system can be identified by a carbon extraction replica technique<sup>17</sup> and electron diffraction.

Other systems amenable to this type of study are, Fe-Zr-O, Fe-Ca-O and Fe-Ti-O. Using the results of this study for the Fe-Si-O system, more complex systems such as Fe-Mn-Si-O, Fe-Cr-Si-O and Fe-S-Si-O might be investigated. The latter system was examined briefly in this study. The inclusions were, in most cases, complex sulphide - silicate mixtures and extremely difficult to identify. The cold-nitric acid extraction technique could not be used as sulphur was partially soluble in the acid. However the inclusions were more massive, especially in the high sulphur ingots, and could be analyzed by electron probe techniques. The sequence of investigations

in this systems would be firstly, to perform solidification studies with simple Fe-S alloys then progress to Fe-S-O combinations and eventually to examine the four component system.

### B. Levitation Studies

Experimental information concerning the supercooling necessary to homogeneously nucleate oxide phases might be obtained from a levitation technique. Iron containing silicon and oxygen could be levitated at high temperatures then cooled above the melting point of iron. The levitation technique eliminates the crucible problem and hopefully, concentrations of oxide nuclei in the liquid, thus necessitating supercooling for nucleation. Slag phases in rapidly stirring levitated melts tend to be surface active and often form a film about the molten metal ball. If this occurred, the onset of nucleation could be detected by a sudden change in the emissivity of the levitated melt.

### C. Zone Refining Studies

The effect of solidification rates on the distributions and nature of inclusions, in particular the rod-like eutectic, might be examined by means of a zone refining study. Zones could be passed through iron bars containing small amounts of silicon and oxygen. The rate of advance of the solid-liquid interface could be carefully controlled and the resulting inclusions examined by the techniques developed in this study.

REFERENCES

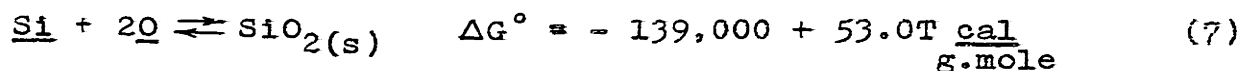
1. C. E. Sims, Transactions A.I.M.E., 215, 367 (1959).
2. M. Baeyertz, Non-metallic Inclusions in Steel, A.S.M., Cleveland, Ohio (1947).
3. A. M. Portevin and R. Perrin, Journal Iron and Steel Institute, 127, 153 (1933).
4. A. M. Portevin and R. Castro, Journal Iron and Steel Institute, 132, 237 (1935); 134, 213 (1936).
5. R. Kiessling and N. Lange, Non-Metallic Inclusions in Steel, The Iron and Steel Institute. Special Report No. 90, (1964).
6. C. Benedicks and H. Lofquist, Non-metallic Inclusions in Iron and Steel, Chapman and Hall, London (1930).
7. C. H. Herty, Jr., Deoxidation of Steel, A Memorial Volume, A.I.M.E. (1957).
8. D. C. Hilty and Walter Crafts, Journal of Metals, 1307 (1952).
9. D. C. Hilty and Walter Crafts, Transactions A.I.M.E., 188, 425 (1950).
10. C. A. Zappfe and C. E. Sims, Transactions A.I.M.E., 154 191 (1943).
11. N. A. Gokcen and J. Chipman, Transactions A.I.M.E., 194 171 (1952), 197 1017 (1953).
12. T. E. Rooney and A. G. Stapleton, Journal Iron and Steel Institute, 131, 249 (1935).
13. E. W. Colbeck, Journal Iron and Steel Institute, 134, 251 (1936).
14. E. L. Evans and H. A. Sloman, Journal Iron and Steel Institute, 172, 296 (1952).
15. W. A. Fischer and M. Wahlster, Archiv fur das Eisenhüttenwesen, 28, 601 (1957); 29, 1 (1958).
16. E. T. Turkdogan, Transactions A.I.M.E., 233, 2100 (1965).

17. M. L. Turpin and J. F. Elliott, *Journal Iron and Steel Institute*, 204, 217 (1966).
18. J. W. Cahn and J. E. Hilliard, *Journal of Chemical Physics*, 28, 258 (1958).
19. D. Turnbull and J. C. Fisher, *Journal of Chemical Physics*, 17, 71 (1949).
20. L. S. Darken and R. W. Gurry, *Journal American Chemical Society*, 68, 798 (1946).
21. N. L. Bowen and J. F. Schairer, *American Journal of Science*, 24, 177 (1932).
22. E. M. Levin, C. R. Robbins and H. F. McMurdie, Phase Diagrams for Ceramists, The American Ceramic Society, (1964).
23. J. F. Elliott, M. Gleiser and V. Ramakrishna, Thermochemistry for Steelmaking, 2, A.I.S.I. (1963).
24. S. Matoba, K. Gunji and T. Kuwana, *Stahl und Eisen*, 80, 299 (1960).
25. L. S. Darken and R. W. Gurry, *Journal American Chemical Society*, 67, 1398 (1945).
26. T. P. Floridis and J. Chipman, *Transactions A.I.M.E.*, 212, 549 (1958).
27. C. Bodsworth and I. M. Davidson, *Physical Chemistry of Process Metallurgy (I)*, Met. Soc. A.I.M.E. Conf. Series 7, 238 (1960).
28. W. G. Pfann, Zone Melting, John Wiley & Sons, New York, (1958).
29. M. T. Hepworth, R. P. Smith and E. T. Turkdogan, "Permeability, Solubility and Diffusivity of Oxygen in B.C.C. Iron", Paper, Annual Meeting, A.I.M.E., New York (1966).
30. B. Chalmers and D. Uhlmann, Principles of Solidification, 228, John Wiley and Sons, New York, (1964).
31. N. A. Gokcen and J. Chipman, *Transactions A.I.M.E.*, 195, 171 (1952).
32. T. F. Bower, H. D. Brody and M. C. Flemings, "Measurements of Solute Redistribution in Dendritic Solidification", December 1 (1965).

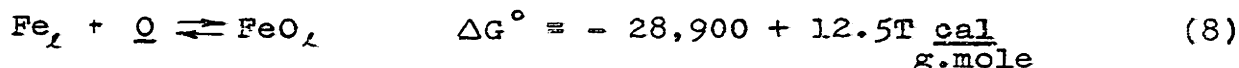
33. D. R. Poirier, Sc.D. Thesis, M.I.T. (1966).
34. Professor J. W. Cahn, Massachusetts Institute of Technology, Private Communication.
35. G. A. Chadwick, Progress in Materials Science, 10, 97 (1963).
36. B. Chalmers, Principles of Solidification, John Wiley & Sons, New York, (1964).
37. B. Chalmers, Physical Metallurgy, John Wiley & Sons, New York, 280 (1959).
38. B. Vonnegut, Journal Colloid Science, 3, 563 (1948).
39. D. Turnbull, Journal Applied Physics, 20, 817 (1949).
40. D. Turnbull, Transactions A.I.M.E., 188, 1144 (1950).
41. V. Danilov and W. Neumark, Physik. Zeits. Sowjet Union., 12, 313 (1937).
42. Y. Miyashita, Nippon Kokan Tech. Report, 4, 41 (1965).
43. C. Zener, Journal of Applied Physics, 20, 950 (1949).
44. N. A. Gokcen and J. Chipman, Transactions A.I.M.E., 197, 173 (1953).
45. D. C. Hilty and W. Crafts, Transactions A.I.M.E., 188, 414 (1950).
46. A. McLean and R. G. Ward, Journal Iron and Steel Institute, 204, 8 (1966).
47. V. Oelsen, K. Sauer and H. Keller, Archiv fur das Eisenhüttenwesen, 7, 529 (1965).
48. C. Wang and C. S. Smith, Transactions A.I.M.E., 188, 136 (1950).

APPENDIX ACALCULATION OF LIQUID IRON COMPOSITIONS IN EQUILIBRIUM WITH  
UNSATURATED FeO-SiO<sub>2</sub> SLAGS

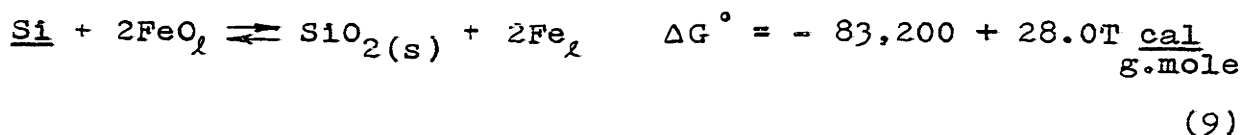
Given,



and



Multiplying equation (8) by two and subtracting from equation (7) one gets,

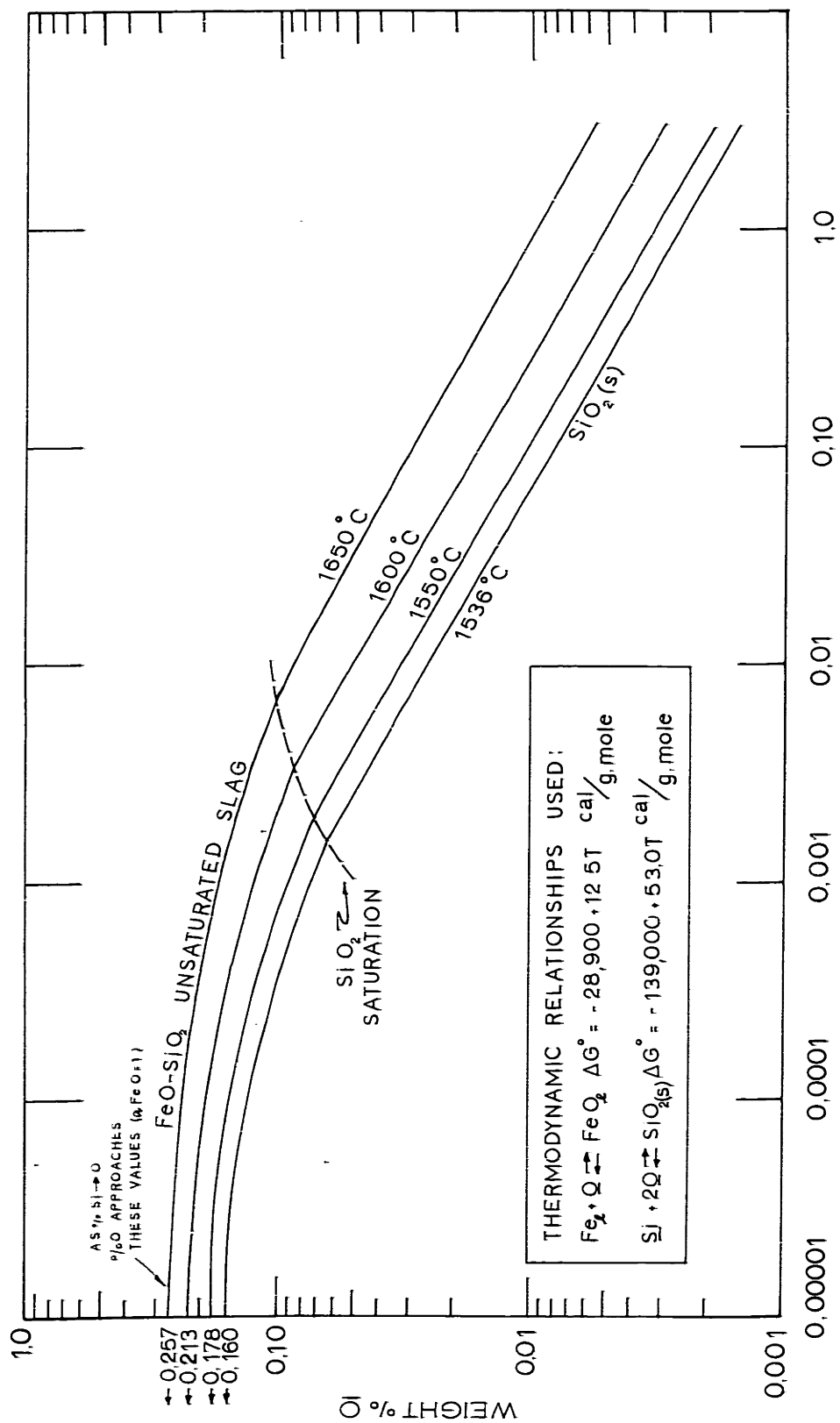


Bodsworth has measured the activities of FeO and SiO<sub>2</sub> in FeO-SiO<sub>2</sub> slags. Thus, for a given slag composition, assuming the activity of iron to be 1.0, the activity of Si in iron in equilibrium with the slag may be calculated from

$$K = \log \frac{a_{\text{SiO}_2} \cdot a_{\text{Fe}}^2}{a_{\text{FeO}}^2 \cdot a_{\text{Si}}} \quad (10)$$

The corresponding oxygen activity was calculated by inserting the calculated Si activity and the measured SiO<sub>2</sub> activity into equation (7). The complete Fe-Si-O equilibrium is shown in Figure A-1.





Si-O Equilibrium in Liquid Iron

FIGURE A-1

APPENDIX BCALCULATION OF FREEZING POINT LOWERING

(Temperature Profile for the line of two-fold saturation in the system Fe-Si-O)

The liquid temperatures were calculated from the expression,

$$T_{\text{liquid}} = 1536^{\circ}\text{C} - 50\%(\%O) - 11.2\%(\%Si)$$

The coefficients for oxygen and silicon were calculated from the binary phase diagrams assuming the liquidus lines to be linear.

Results:

0.002%Si:	$T_{\ell} = 1536^{\circ}\text{C} - 50(0.056) - 11.2(0.002) = 1533.2^{\circ}\text{C}$
0.01%Si:	$T_{\ell} = 1536^{\circ}\text{C} - 50(0.025) - 11.2(0.01) = 1534.7^{\circ}\text{C}$
0.04%Si:	$T_{\ell} = 1536^{\circ}\text{C} - 50(0.013) - 11.2(0.04) = 1534.9^{\circ}\text{C}$
0.10%Si:	$T_{\ell} = 1536^{\circ}\text{C} - 50(0.008) - 11.2(0.10) = 1534.5^{\circ}\text{C}$
0.20%Si:	$T_{\ell} = 1536^{\circ}\text{C} - 50(0.007) - 11.2(0.20) = 1533.5^{\circ}\text{C}$
1.0%Si:	$T_{\ell} = 1536^{\circ}\text{C} - 50(0.0026) - 11.2(1.0) = 1524.7^{\circ}\text{C}$

APPENDIX CTHE CHEMICAL ISOLATION AND ANALYSIS OF OXIDE INCLUSIONSA. PROCEDURE

The ingot to be analyzed was carefully filed to remove any pieces of crucible or slag adhering to its edges. One to six grams of fine turnings, the amount depending on the anticipated weight of residue, were prepared from the sample. The turnings were weighed then added to 100 milliliters of diluted nitric acid (5 vol.  $\text{HNO}_3$  + 1 vol.  $\text{H}_2\text{O}$ ) which had been cooled to  $2^\circ\text{C}$  by the addition of crushed dry ice. During dissolution the turnings were strongly agitated with a magnetic stirrer. The temperature was measured with an immersed thermometer and was kept in the range  $2^\circ - 7^\circ\text{C}$  by the periodic addition of crushed dry ice. The dissolution time varied from ten to forty minutes. The completion of the dissolution process was indicated when the last of the turnings had disappeared from the magnetic stirrer. At this point the solution was stirred an extra ten minutes to ensure that all of the turnings had dissolved.

Often during the dissolution process iron nitrate would precipitate halting the reaction. The addition of 10 to 20 milliliters of cold distilled water cleared the solution and allowed the reaction to continue.

After dissolution the solution was passed through a membrane filter having a pore diameter of  $0.3\mu$ . The filter paper, suction flask and attachments were supplied by the

Millipore Company of Malden, Massachusetts. Before filtration the filter paper was moistened with cold distilled water.

After filtration the filter and the residue were washed with 100 milliliters of  $\text{HNO}_3$  solution (5 + 1) previously cooled to  $2^\circ\text{C}$  with dry ice.

When filtration was complete the filter flask walls and the magnetic stirrer were wiped with a clean filter paper to remove any oxide particles. This paper was carefully folded together with the membrane filter and the whole placed in a platinum crucible for ignition.

The ignited residue was then weighed and analyzed for silicon or iron. The results of the analyses together with calculated total oxygen contents and vacuum fusion results are shown in Table C-1.

#### B. DISCUSSION OF RESULTS

The total oxygen contents of the ingots determined by the extraction method compare favorably with those determined by vacuum fusion and by equilibrium calculations. Discrepancies appear in the high silicon or low oxygen ingots. The reason for this divergence is due partly to the extremely small residue weights. For example, for ingot number 58 containing 0.342 Wt% Si, an oxide residue of 0.60 milligrams was obtained from an initial sample weighing 2.38 grams. On the other hand an oxide residue of 3.5 milligrams resulted from the dissolution of only 1.00 gram of ingot number 98 containing 0.011 Wt% Si.

TABLE C-1: RESULTS OF EXTRACTION AND ANALYSIS OF INCLUSIONS

No.	Total Si (Wt%)	Sample Weight (gms)	Residue Weight (mgs)	Iron in Residue (mgs)	Si in Residue (mgs)	Wt% as FeO	Wt% as SiO <sub>2</sub>	Wt% total	Wt% Vac. Fusion	Wt% Eq'm Calc.	% of total as SiO <sub>2</sub>
104	0.004	3.95 3.93	12.50 12.30	8.15	0.08	0.0595	0.0026	0.062		0.042	4.16
107	0.005	3.00 3.00	9.20 8.60	6.01	0.07	0.0555	0.0026	0.058		0.038	4.54
114	0.006	1.52 1.52	4.30 3.80	2.96	0.058	0.0525	0.0043	0.057	0.061	0.033	7.60
99	0.006	1.53 1.51 1.50 1.50	4.60 4.1 4.00 3.90	2.45 2.45	0.065 0.055	0.043	0.0045	0.048		0.033	9.5
113	0.007	1.53 1.53	2.10 1.70	1.30	0.066	0.022	0.0049	0.027		0.031	18.0
108	0.008	2.01 2.08	6.30 6.50	4.20	0.120	0.0572	0.0068	0.064		0.029	10.6
98	0.011	1.00 1.00 1.00 1.00	3.50 3.10 3.50 3.50	1.98 2.08 2.03	0.085	0.0543	0.010	0.064	0.074	0.025	15.5
54	0.016	2.50 2.50 2.50 2.39	1.00 1.60 1.40 1.10	0.65 0.35	0.192 0.155	0.0046	0.008	0.013		0.021	63.0
109	0.016	3.03 3.03	1.70 2.00	0.865	0.236	0.0053	0.0089	0.014	0.024	0.021	63.0
101	0.017	2.04 2.00	1.40 1.70	0.590	0.180	0.0057	0.010	0.016		0.020	64.0

TABLE C-1 (CONT'D): RESULTS OF EXTRACTION AND ANALYSIS OF INCLUSIONS

No.	Total Si (Wt%)	Sample Weight (gms)	Residue Weight (mgs)	Iron in Residue (mgs)	Si in Residue (mgs)	Wt% as FeO	Wt% as SiO <sub>2</sub>	Wt% total	Wt% Vac. Fusion	Wt% Eq'm Calc.	% of total as SiO <sub>2</sub>
105	0.040	2.84	1.60		0.360		0.014	0.018	0.014	0.013	82.0
		2.84	1.90	0.60		0.0033					
55	0.075	1.75	0.65		0.156		0.010	0.010		0.010	100.0
		1.68	0.60	0.156	0.152						
		1.76	0.60	0.168							
57	0.126	1.64	0.70		0.110		0.0076	0.008	0.007	0.007	93.0
		1.64	0.80	0.200		0.0006					
60	0.76	2.06	0.70		0.150		0.0096	0.0010		0.006	100.0
		2.11	0.80	0.196	0.205						
		1.92	0.80	0.288							
		2.20	0.70								
63	0.211	2.79	0.80		0.137		0.0065	0.006		0.006	100.0
		2.70	0.70	0.140	0.179						
		2.70	0.70	0.160							
		2.75	0.80								
58	0.342	2.45	0.65		0.131		0.0057	0.006		0.004	89.1
		2.35	0.55	0.248	0.111						
		2.38	0.60	0.372							
64	0.702	1.70	0.40		0.075		0.005	0.005	0.002	0.003	100.0
		1.64	0.80	0.23							

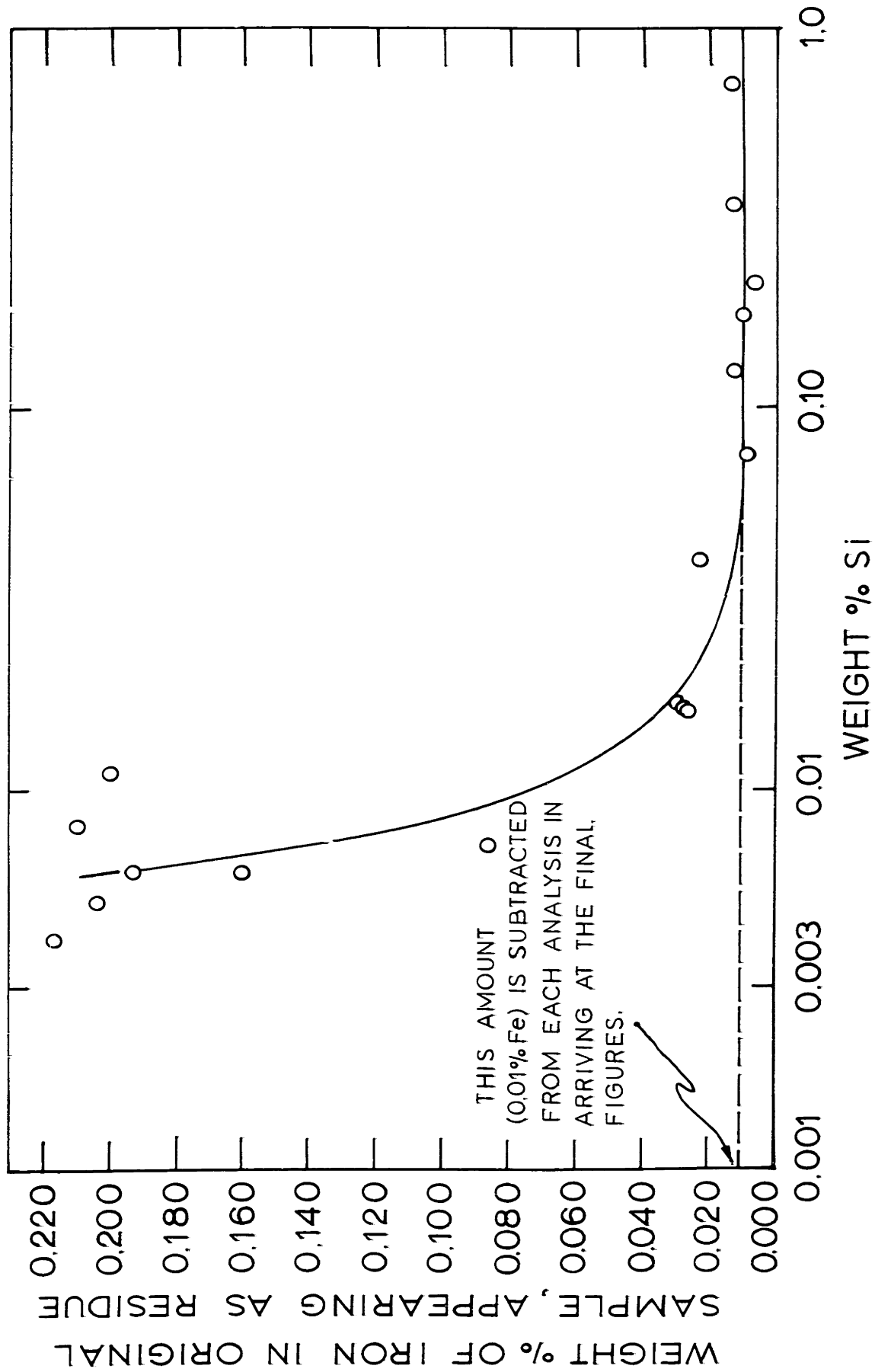
Thus, if there was a minute and constant amount of insoluble iron or iron nitrate present in both residues then the results from the high silicon ingot would be more in error than those of the low silicon ingot. One is to recall that from the iron analysis of the residue that the oxygen associated with this iron is assumed to be FeO.

An indication of this effect in the high silicon ingots was the fact that the residue silicon analysis, and hence the total oxygen present as SiO<sub>2</sub>, more than accounted for the total oxygen present as indicated by the vacuum fusion.

An estimate of the amount of "extraneous" iron in the oxide residues was made by plotting

$$\frac{\text{weight of Fe in residue}}{\text{weight of original sample}} \times 100$$

versus percent silicon. This is shown in Figure C-1.



Estimation of Amount of Extraneous Iron in Oxide Residues

FIGURE C-1



The percent of the original iron present in the residue drops rapidly in the range 0.01 to 0.07 Wt% Si and levels off at a value of 0.01 Wt% with higher silicon values.

If this constant amount of iron were indeed due to the presence of FeO formed from deoxidation reactions then the FeO / SiO<sub>2</sub> ratio would reach a minimum at 0.10 Wt% Si and increase rapidly with increasing silicon content. This behaviour is in disagreement with thermodynamic considerations and with observations of other workers.

Several quantitative NO<sub>3</sub><sup>-</sup> analyses were performed on the residues which indicated that sufficient NO<sub>3</sub><sup>-</sup> ion was present to account for the constant amount of iron as insoluble Fe(NO<sub>3</sub>)<sub>3</sub> · x 6H<sub>2</sub>O. This analysis is not conclusive however as the NO<sub>3</sub><sup>-</sup> ion might easily be that associated with traces of HNO<sub>3</sub> contained in the filter.

In light of the above considerations it was assumed that 0.01 Wt% of the original iron sample appeared in the residue as either Fe(NO<sub>3</sub>)<sub>3</sub> · x 6H<sub>2</sub>O or as insoluble iron. This amount of iron was subtracted from the iron residue analysis in arriving at a value for iron present as FeO.

APPENDIX DX-RAY DIFFRACTION OF OXIDE RESIDUES

Sample No. 103; Si = 0.002 wt%

Sample Preparation: The residue was scraped from a millipore filter and placed on a glass slide. A glass fiber was rotated in the residue then placed in the chamber of the Debye Scherrer camera.

X-Ray Conditions: Chromium radiation using an iron filter at 35KV and 15mA for one and one half hours.

Index:

<u>Film</u>					<u>FeO ASTM Card 6-0615</u>		
line	$\theta^\circ$	$\sin \theta / \lambda$	1/d	$d_A^\circ$	$d_A^\circ$	I/I	hkl
1	27.63	0.200	0.400	2.50	2.486	80	111
2	32.40	0.234	0.468	2.14	2.153	100	200
3	49.20	0.330	0.660	1.52	1.523	60	220
4	62.35	0.390	0.780	1.28	1.299	25	311
5	67.38	0.400	0.800	1.25	1.243	15	222

Identification: FeO

APPENDIX ELOT ANALYSIS OF ELECTROLYTIC IRON

(Plastiron from Plastic Metals Corporation)

<u>Wt%</u>			<u>Wt%</u>
Al	0.002	Mo	0.002
A	Nil	Ni	0.030
C	0.002	N	0.004
Cr	0.002	O	0.0070
Co	0.007	P	0.005
Cu	0.008	Si	0.005
H	0.010	S	0.004
Pb	Nil	Sn	0.005
Mg	0.002	Va	0.003
Hg	Nil		

APPENDIX FINCLUSION AREA COUNT  
(WITH QUANTITATIVE TELEVISION MICROSCOPE)

Procedure: Inclusion area counts of random spheres were performed on several ingot sections. Spot counts were taken progressing from ingot top to bottom. Results for three ingots are given below.

Results:

	<u>No. 125 (1550°C)</u> <u>(area %)</u>	<u>No. 126 (1650°C)</u> <u>(area %)</u>	<u>No. 127 (1650°C)</u> <u>(area %)</u>
Top	0.14	0.19	0.10
	0.05	0.11	0.01
	0.04	0.21	-
	0.07	0.16	-
	0.13	0.08	trace
	0.10	0.11	-
	0.01	0.16	-
	0.01	0.10	trace
	0.02	0.14	-
	0.01	0.24	-
	0.02	0.22	-
	0.03	0.03	-
Bottom	<u>0.01</u>	<u>0.10</u>	<u>-</u>
Average	0.04%	0.14%	0.00%

Table F-1: Results of Inclusion Counts for Ingots 125, 126 and 127 Performed on a Quantitative Television Microscope.

BIOGRAPHICAL NOTE

The author was born in Vancouver, British Columbia, Canada on July 15, 1936. He attended the University of British Columbia where he received the degree of Bachelor of Applied Science in Metallurgical Engineering in 1960.

In 1962 he received the Master of Applied Science degree in Chemical Metallurgy from the same institution. The title of his thesis for this degree was "The Excess Properties of Copper Cations in  $\text{PbO-Cu}_2\text{O-SiO}_2$  Slags". This work was prepared as a paper and was presented by the author at the A.I.M.E. February meeting in New York in 1964.

From March 1962 to September 1963 he worked as research engineer with the Société de l'Electro Chimie et de l'Electro Metallurgie et des Aciers Electriques d'Ugine in Lyons, France.

He has since been a candidate for the degree of Doctor of Science at the Massachusetts Institute of Technology with a major in Metallurgy and a minor in Industrial Management.

BIOGRAPHICAL NOTE

in Vancouver, British Columbia,  
attended the University of  
received the degree of Bachelor of  
Electrical Engineering in 1960.

received the Master of Applied Science  
from the same institution. The  
thesis degree was "The Excess Properties  
of  $SiO_2$  Slags". This work was  
presented by the author at the  
American Chemical Society in New York in 1964.

In September 1963 he worked as  
assistant at the Société de l'Electro Chimie et de  
Machines Electriques d'Ugine in

candidate for the degree of  
Massachusetts Institute of Technology  
with a minor in Industrial Management.







